

CONFORMATIONS AND PERMEATION MECHANISM INTO LIPID BILAYER
OF CYCLODEXTRINS

Miss Wasinee Khuntawee



จุฬาลงกรณ์มหาวิทยาลัย

CHULALONGKORN UNIVERSITY

บทคัดย่อและแฟ้มข้อมูล ตั้งแต่ของวิทยานิพนธ์ตั้งแต่ปีการศึกษา 2554 ที่ให้บริการในคลังข้อมูลภาษา (CUIR)

A Dissertation Submitted in Partial Fulfillment of the Requirements
for the Degree of Doctor of Philosophy Program in Nanoscience and Technology

(Interdisciplinary Program)

The abstract and full text of theses from the academic year 2011 in Chulalongkorn University Intellectual Repository (CUIR)

are the thesis authors' files submitted through the University Graduate School.

Graduate School

Chulalongkorn University

Academic Year 2015

Copyright of Chulalongkorn University

คอนฟอร์เมชันและกลไกการนำเข้าสู่ลิพิดแบบแผ่นสองชั้นของไซโคลเดกซ์ทริน

นางสาววาสนิ ขุนทวี



วิทยานิพนธ์นี้เป็นส่วนหนึ่งของการศึกษาตามหลักสูตรปริญญาวิทยาศาสตรดุษฎีบัณฑิต

สาขาวิชาวิทยาศาสตร์นาโนและเทคโนโลยี (สหสาขาวิชา)

บัณฑิตวิทยาลัย จุฬาลงกรณ์มหาวิทยาลัย

ปีการศึกษา 2558

ลิขสิทธิ์ของจุฬาลงกรณ์มหาวิทยาลัย

Thesis Title	CONFORMATIONS AND PERMEATION MECHANISM INTO LIPID BILAYER OF CYCLODEXTRINS
By	Miss Wasinee Khuntawee
Field of Study	Nanoscience and Technology
Thesis Advisor	Professor Supot Hannongbua, Dr.rer.nat.
Thesis Co-Advisor	Thanyada Rungrotmongkol, Ph.D. Assistant Professor Jirasak Wong-ekkabut, Ph.D.

Accepted by the Graduate School, Chulalongkorn University in Partial
Fulfillment of the Requirements for the Doctoral Degree

..... Dean of the Graduate School
(Associate Professor Sunait Chutintaranond, Ph.D.)

THESIS COMMITTEE

..... Chairman
(Associate Professor Vudhichai Parasuk, Ph.D.)

..... Thesis Advisor
(Professor Supot Hannongbua, Dr.rer.nat.)

..... Thesis Co-Advisor
(Thanyada Rungrotmongkol, Ph.D.)

..... Thesis Co-Advisor
(Assistant Professor Jirasak Wong-ekkabut, Ph.D.)

..... Examiner
(Professor Piamsook Pongsawasdi, Ph.D.)

..... Examiner
(Associate Professor Warangkana Warisnoicharoen, Ph.D.)

..... Examiner
(Rattapol Rangkupan, Ph.D.)

..... External Examiner
(Assistant Professor Ornjira Aruksakunwong, Ph.D.)

วาสิณี ขุนทวี : คอนฟอร์เมชันและกลไกการนำเข้าสู่ลิพิดแบบแผ่นสองชั้นของไซโคลเดกซ์ทริน (CONFORMATIONS AND PERMEATION MECHANISM INTO LIPID BILAYER OF CYCLODEXTRINS) อ.ที่ปรึกษาวิทยานิพนธ์หลัก: ศ. ดร. สุพจน์ หารหนองบัว, อ.ที่ปรึกษาวิทยานิพนธ์ร่วม: ดร. ธัญญดา รุ่งโรจน์มงคล, ผศ. ดร. จิรศักดิ์ วงศ์เอกบุตร, 96 หน้า.

ไซโคลเดกซ์ทรินคือ โมเลกุลโฮสต์ที่มีศักยภาพในการปรับปรุงสมบัติทางกายภาพและทางเคมีของสารประกอบเกสต์ โดยผ่านการเกิดสารประกอบเชิงซ้อนของสารเหล่านั้น การยึดจับและการไม่ยึดจับของลิแกนด์เกสต์กับไซโคลเดกซ์ทริน รวมทั้งการปลดปล่อยลิแกนด์เข้าไปในเยื่อหุ้มเซลล์เป็นปัจจัยสำคัญที่ควบคุมฟังก์ชันของสารประกอบเชิงซ้อนไซโคลเดกซ์ทริน ในงานวิจัยเรามีจุดประสงค์เพื่อเข้าใจขั้นตอนก่อนการเกิดสารประกอบเชิงซ้อนไซโคลเดกซ์ทริน ในงานส่วนแรก เราได้ศึกษาความหลากหลายเชิงโครงสร้างของ CD6-CD10 และ CD14 โดยใช้วิธีการจำลองพลวัตเชิงโมเลกุลแบบ replica exchange (REMD) ของโมเลกุลไซโคลเดกซ์ทรินอิสระในสารละลาย ภายใต้สมมติฐานที่ว่า การเปลี่ยนแปลงเชิงโครงสร้างไซโคลเดกซ์ทรินส่งผลต่อประสิทธิภาพการยึดจับของลิแกนด์ เราได้ใช้การจำลองแบบ REMD กับไซโคลเดกซ์ทรินวงใหญ่เป็นครั้งแรก โดยใช้ข้อมูลฟอสไฟด์ของคาร์โบไฮเดรตต่างชนิดกัน และได้ศึกษาสมบัติเชิงโครงสร้างและสมบัติเชิงพลวัตที่เกี่ยวข้องกับการเปลี่ยนแปลงของอนุหุมิ จากผลการทดลองพบว่า *i*) เทคนิค REMD สามารถใช้ในการอธิบายการเปลี่ยนแปลงโครงสร้างของไซโคลเดกซ์ทริน *ii*) ข้อมูลฟอสไฟด์ glycam06 ให้ผลการจำลองที่น่าเชื่อถือ โดยสามารถอธิบายการบิดของหน่วยย่อยของกลูโคสได้ *iii*) โครงสร้างที่พบมากที่สุดของ CD10 และ CD14 เป็นรูปทรงโค้งงอ เช่นเดียวกับโครงสร้างผลึกของสารเหล่านั้น อย่างไรก็ตาม CD14 มีลักษณะที่เปิดออกเล็กน้อยเมื่อเทียบกับโครงสร้างเอ็กซ์เรย์ *iv*) นอกจากนี้ โครงสร้างที่หลากหลายของไซโคลเดกซ์ทรินถูกค้นพบที่อุณหภูมิสูง เนื่องจากวงมีความยืดหยุ่นมากกว่า ในงานส่วนที่สอง เราได้ศึกษาและอธิบายขั้นตอนก่อนการนำส่งลิแกนด์เข้าสู่เมมเบรน โดยการนำส่งในลักษณะการเกิดสารประกอบเชิงซ้อนกับไซโคลเดกซ์ทริน ด้วยการจำลองพลวัตเชิงโมเลกุลในระดับไมโครสเกลของระบบการจำลองพฤติกรรมและการแทรกผ่านของบีตาไซโคลเดกซ์ทรินอิสระเข้าสู่ลิพิดแบบแผ่นสองชั้น จากผลการทดลองพบว่าบีตาไซโคลเดกซ์ทรินแพร่ผ่านเข้าสู่ลิพิดแบบแผ่นสองชั้น โดยหันด้านขอบกว้างเข้าหาหมู่ที่มีขั้วของลิพิด และคงอยู่ระหว่างหมู่ฟอสเฟตกับหมู่กลีเซอรอล-เอสเทอร์ โดยการเกิดพันธะไฮโดรเจน นอกจากนี้ อนุพันธ์ของบีตาไซโคลเดกซ์ทริน (เมทิลเลด- และ 2-ไฮดรอกซีโพรพิล เบต้าไซโคลเดกซ์ทริน) แสดงการแทรกผ่านที่ลึกกว่า ซึ่งอาจสามารถอธิบายถึงสาเหตุที่อนุพันธ์ของบีตาไซโคลเดกซ์ทรินทั้งสองชนิด ทำให้เกิดการปลดปล่อยลิแกนด์ที่ไม่ชอบน้ำได้เร็วกว่า จากการค้นพบในงานวิจัยนี้อาจเป็นประโยชน์ในการเลือกไซโคลเดกซ์ทรินที่เหมาะสมในการนำส่งยาและการออกแบบตัวนำส่งยาที่มีประสิทธิภาพสูงต่อไป

สาขาวิชา วิทยาศาสตร์นาโนและเทคโนโลยี
ปีการศึกษา 2558

ลายมือชื่อนิติกร
ลายมือชื่อ อ.ที่ปรึกษาหลัก
ลายมือชื่อ อ.ที่ปรึกษาร่วม
ลายมือชื่อ อ.ที่ปรึกษาร่วม

5487846820 : MAJOR NANOSCIENCE AND TECHNOLOGY

KEYWORDS: CLYCLODEXTRIN / MOLECULAR DYNAMICS SIMULATION / REPLICA EXCHANGE / CONFORMATION / LIPID / PERMEATION

WASINEE KHUNTAWEE: CONFORMATIONS AND PERMEATION MECHANISM INTO LIPID BILAYER OF CYCLODEXTRINS. ADVISOR: PROF. SUPOT HANNONGBUA, Dr.rer.nat., CO-ADVISOR: THANYADA RUNGROTMONGKOL, Ph.D., ASST. PROF. JIRASAK WONG-EKKABUT, Ph.D., 96 pp.

Cyclodextrins (CDs) are potent host molecules, which can improve physical and chemical properties of guest compounds through their inclusion complexes. The binding and unbinding between guest ligand and CDs as well as the releasing into cell membrane are key factors that control the CD complex functions. Here, we aim to understand the pre-steps of that CD-ligand formation. Firstly, the conformational diversity of CD6-CD10 and CD14 was studied by the replica exchange molecular dynamics (REMD) simulations. Free CD molecules in solution were performed under the assumption that the CDs structural changes may influence the ligand binding affinity. The large ring CD (LR-CD) systems were tested for the first time with REMD simulations using various carbohydrate force fields. The structural properties and the dynamic behavior of LR-CDs corresponding to temperature changes were newly investigated. Our results indicate that: *i*) REMD simulation can describe the CDs conformational changes, *ii*) the glycam06 force field is reliable for describing the flip of glucose subunits, *iii*) the most probable conformations of CD10 and CD14 are bent-shape like their crystals, however, CD14 is slightly opened in comparison to the X-ray structure, *iv*) additionally, the various conformations of CDs could be also observed at high temperatures due to their high ring flexibility. Secondly, the pre-step of ligand transportation based on CD inclusion complexes into the membrane was studied. The micro-scale molecular dynamics (MD) simulations were used to investigated the permeation behavior of single beta-cyclodextrin (β CD) into lipid bilayer. Our results show that β CD passively diffuses into the lipid bilayer by pointing its wider rim toward the lipid polar groups and then remains at the phosphate and glycerol-ester groups with hydrogen bond formation. Moreover, the β CD derivatives (methylated- and hydroxypropyl- β CD) showed a somewhat deeper permeation that might be able to explain why these two derivatives offer a faster release of hydrophobic ligands. Our findings in this study might be helpful for the selection of proper CDs for drug transport as well as for further design of higher potent drug carriers.

Field of Study: Nanoscience and Technology

Academic Year: 2015

Student's Signature

Advisor's Signature

Co-Advisor's Signature

Co-Advisor's Signature

ACKNOWLEDGEMENTS

Firstly, I would like to thank the Nanoscience and Technology Program, Graduate School and also the Center of Innovative Nanotechnology (CIN), Chulalongkorn University for give me a good chance and experiences including continuous funding support of my Ph.D study.

I would like to express my sincere gratitude to my advisor, Professor Supot Hannongbua, Dr. rer. nat. for presenting an opportunity, valuable suggestions and for his help during the course of this research. I am very thankful to my co-advisor, Dr. Thanyada Rungrotmongkol for her kind assistance and teaching, not only the research idea but also many other ideas. I would like to give very special thanks to Asst. Prof. Dr. Jirasak Wong-ekkabut, my thesis co-advisor for share me on his excellent research experiences on membrane simulations, support and guidance help in all the time.

Besides my advisors, I would like to thank the rest of my thesis committee: Assoc. Prof. Dr. Vudhichai Parasuk, Prof. Dr. Piamsook Pongsawasdi, Assoc. Prof. Dr. Warangkana Warisnoicharoen, Dr. Ratthapol Rangkupan and Asst. Prof. Dr. Ornjira Aruksakunwong for their comments, suggestions and encouragement.

I am thankful to Prof. Dr. Peter Wolschann, Department of Pharmaceutical Technology and Biopharmaceutics, University of Vienna for his kind suggestions about cyclodextrin research including this thesis writing and give me very nice experiences during my visit of his laboratory in Vienna. My sincere thanks also goes to Assoc. Prof. Dr. Hisashi Okumura, Department of Structural Molecular Science, The Graduate University for Advanced Studies, Japan who provided me an opportunity to visit his laboratory and teaching me in particular the replica exchange MD method. I am also very grateful to Dr. Manaschai Kunaseth, National Nanotechnology Center (NANOTEC) for sharing his structural analysis programs in the conformation study of CD14.

All members of Computational Chemistry Unit Cell (CCUC), Chulalongkorn University are also acknowledged for very nice friendship and all kind helps. The Computer Chemistry Unit Cell, the Vienna Scientific Cluster (VSC-2) and Computational Biophysics Group, Department of Physics, Faculty of Science, Kasetsart University are acknowledged for facility and computing resources.

I would like to thank the National Research Council of Thailand, the 90th anniversary of Chulalongkorn University fund and Ratchadaphiseksomphot Endowment Fund for financial supports.

Lastly, I would like to thank my parents and my family, for encouraging and understanding me for my study. I would not have achieved this far and this thesis would not have been completed without all the support that I have always received from them.

CONTENTS

	Page
THAI ABSTRACT	iv
ENGLISH ABSTRACT.....	v
ACKNOWLEDGEMENTS.....	vi
CONTENTS.....	vii
TABLES LIST	ix
FIGURES LIST	x
CHAPTER 1 INTRODUCTION	1
1.1) Cyclodextrins (CDs)	2
1.2) Biological membrane	9
1.3) Molecular dynamics (MD) technique	10
1.4) Research rational.....	12
1.5) Research objectives.....	13
CHAPTER 2 THEORETICAL BACKGROUND.....	14
2.1) Molecular Dynamics (MD) simulation	14
2.1.1) Equation of motion.....	14
2.1.2) Numerical integration	16
2.1.3) Potential function	18
2.2) Temperature Replica Exchange Molecular Dynamics (T-REMD).....	20
CHAPTER 3 METHODOLOGY	23
3.1) Part I: Conformational diversity of cyclodextrins	23
3.2) Part II: Study of permeation mechanism of beta cyclodextrin and its derivatives through the biological membrane	25
CHAPTER 4 RESULTS AND DISCUSSIONS.....	29
4.1) Part I: Conformational diversity of cyclodextrins	29
4.1.1) Validation of REMD simulation setup.....	29
4.1.2) The conformation change of CD10.....	38
4.1.3) The conformation change of CD14.....	46

	Page
4.2) Part II: Study of permeation mechanism of beta cyclodextrin and its derivatives to the biological membrane.....	56
4.2.1) The permeation and insertion of β CD into the lipid bilayer	57
4.2.2) The interaction of β CD with the lipid bilayer.....	64
4.2.3) The conformation of the β CD change in lipid bilayer	68
4.2.4) The influence of chemical modification of β CD on membrane permeability	70
CHAPTER 5 CONCLUSIONS	75
REFERENCES	78
APPENDIX.....	93
VITA.....	96



TABLES LIST

Table 1.1 Physicochemical properties of LR-CDs compared with those of SR-CDs	8
Table 3.1 Details of focused β CD models	26
Table 4.1 The focused structural properties, d_1 [O2-O3'], d_2 [O4-O4'], d_3 [O2-O6'], d_4 [O3-O6'], d_5 [O3-O5'] and τ [O2-C1-C4'-O3'] measured from the crystal structure of CD10	39
Table 4.2 Structure properties of classified CD10 conformations as considering the number of turns angle (θ), the d_1 [O2-O3'], d_2 [O4-O4'], θ [C6-C2'-C6'] and τ [O2-C1-C4'-O3'] of each connecting unit are compared with X-ray	42
Table 4.3 The probability distribution of CD10 conformation with different number of turns and the thermodynamics quantities ΔF , ΔE , and $T\Delta S$ at 300K ...	46
Table 4.4 Average values of the focused parameters on β CD-lipid interactions for all simulations (BCD1-BCD5) over the MD production period.....	63
Table 4.5 The RMSD and cavity area of β CD molecule on each hydroxyl rim....	70

FIGURES LIST

Figure 1.1 Number of publications and patents on cyclodextrin in the past 15 years	2
Figure 1.2 Distribution of the publications and patents among the fields of CD applications	2
Figure 1.3 (Left) Top and (right) side views of 2D structure of β CD and its derivatives, methylated- β CD and 2-hydroxypropyl- β CD.	4
Figure 1.4 Illustration of crystal structures for CD10, CD14 and CD26	6
Figure 1.5 (a) Common features of plasma membrane containing three main components as phospholipids, proteins and carbohydrates and (b) The structure pattern of 1-palmitoyl-2-oleoyl-sn-glycero-3-phosphocholine (POPC) phospholipid	10
Figure 1.6 (a) Example of phospholipids and (b) Distribution of phospholipids in various parts of mammalian cell	10
Figure 2.1 A standard molecular dynamics simulation algorithm, e.g. as implemented in GROMACS	15
Figure 2.2 Typical molecular mechanics interactions used in GROMACS	19
Figure 2.3 The ideal of temperature replica exchange MD simulation	21
Figure 2.4 Comparison between the structural analysis of classical MD and replica exchange MD	22
Figure 3.1 Overview of research project.....	23
Figure 3.2 (a)-(c): Starting geometries of various orientations β CD at the membrane surface (d)-(e): Starting geometries of various orientations β CD inside the membrane.....	27
Figure 4.1 Top- and side-view of CD10 X-ray structure, a helical band subunit is shown with five glucose rings as presented in bold sticks.....	30
Figure 4.2 The probability distributions of the total potential energy for the REMD simulations with the three solvation models Igb1, Igb2 and Igb5.....	30
Figure 4.3 (a) CD fragment showing the atomic labels and focused structural parameters, d_1 [O2-O3'], d_2 [O4-O4'], d_3 [O2-O6'], d_4 [O3-O6'], d_5 [O3-O5'] and τ [O2-C1-C4'-O3']. A turn between two glucose units is shown for the left glucose	

unit, whereas the two other glucose rings are within the band structure in <i>cis</i> position.....	31
Figure 4.4 Contour plots of the probability distribution of overall snapshots of CD10 with the three different force fields (glycam04, glycam06 and q4md-CD force fields)	32
Figure 4.5 Contour plots of the probability distribution of overall snapshots of CD10 with the three different solvation models, Igb1, Igb2, and Igb5 at 300 K ..	33
Figure 4.6 The Igb1 contour plots of the probability distribution from the 50-ns REMD simulations of CD10 at temperatures 300-600 K.....	34
Figure 4.7 The Igb2 contour plots of the probability distribution from the 50-ns REMD simulations of CD10 at temperatures 300-600 K.....	35
Figure 4.8 The Igb5 contour plots of the probability distribution from the 50-ns REMD simulations of CD10 at temperatures 300-600 K.....	36
Figure 4.9 Contour plots of the probability distribution of CD6-CD10 and CD14 REMD simulations at 300 K.....	37
Figure 4.10 Contour plots of the probability distribution of overall snapshots of CD10 at various temperatures using Igb5 solvent model and glycam06 force field	40
Figure 4.11 Probability of turn rotation of glucose units in CD10 ring at various temperatures.....	44
Figure 4.12 Examples for CD10 conformations with different numbers of turns, extracted from REMD simulation at 300 K.....	44
Figure 4.13 schematic diagram depicting the representative plane P_i (showed in purple color) of one atom cluster (purple cloud on the right), two-most dominant principle axes (v_1 and v_2), and v_{norm} as a normal vector to plane P_i	48
Figure 4.14 Schematic diagram depicting the ratio between the major and minor diameters of the ellipse on a 2D plane.....	49
Figure 4.15 Examples for CD14 structures with various biplanar angle; $\theta_p(1)$ - $\theta_p(9)$, extracted from REMD simulation at 300 K	50
Figure 4.16 Superimposition of 10 MD snapshots of CD14 at 300 K according their circularity change; $\gamma_c^2(1)$ - $\gamma_c^2(10)$	51
Figure 4.17 The thermodynamics quantities ΔF , ΔE , and $T\Delta S$ at 300K of CD14 conformations	52

- Figure 4.18 Distribution plots of (a) biplanar angle (θ_P) and (b) circularity (γ_c^2) for all designed temperatures..... 53
- Figure 4.19 2D contours between the θ_P and γ_c^2 where the probabilities of CD14 in each region are labeled with blue to red color for low to high value, the 16 sampling area is remarked in 2D plot of 300K, defined by S1-S16. 54
- Figure 4.20 Superimposition of the 10 representative MD snapshots in each possible CD14 conformation (S1-S16) i.e. S11 is the most probable CD14 conformations (opened-form), S1 and S5 are closed-form, S3, S4, S8 and S12 are asymmetric bent form, and S13-S14 are 2-loops-like form..... 54
- Figure 4.21 Temperature dependence of CD14 in each conformation S1-S16..... 56
- Figure 4.22 (a) Definition of analysis parameters; $r_{\beta CD}$, $r_{P\beta CD}$, $r_{S\beta CD}$ and (b) vector \vec{r} for tilt angle calculation 58
- Figure 4.23 Closed-up for the first 350 ns of the permeation of βCD into the lipid bilayer for four simulations (BCD1-BCD4) using different initial structures. The distances as a function of time between the centers of bilayer and both rims of βCD molecule *i.e.* primary rim; $r_{P\beta CD}$ (blue) and secondary rim; $r_{S\beta CD}$ (red) are depicted. The βCD tilt angle and the distances of phosphate groups from the center of bilayer for both leaflets (r_P) are plotted in gray and green, respectively. The snapshots of βCD at different simulation time are enclosed in the plots where the blue and red balls represent the atoms of the primary and secondary rims, respectively. The lipids of the bilayer are shown by purple rods while their phosphorus atoms are depicted in green balls. The black and red arrows indicate the approaching and permeating time of βCD to the bilayer, respectively. 59
- Figure 4.24 The association behavior of βCD on POPC bilayer of BCD1-BCD5 system for the whole simulation 60
- Figure 4.25 The last snapshots of BCD1-BCD4 simulations were extracted at 1 μs . The primary rim of βCD , secondary rim of βCD , phosphorus atoms of lipid and water molecules are presented by blue, red, green and cyan spheres, respectively. The purple lines represent the POPC lipid molecules. 62
- Figure 4.26 (a) Dynamics behavior of βCD starting from the perpendicular orientation in the lipid bilayer (BCD5). (b) Water pore formation induced by βCD at longer simulation time, where the cyan sphere represents the water molecules, while the blue, red and green spheres are symbolized as the atoms on primary and secondary rims of βCD and phosphorus of lipid head groups, respectively. 64

- Figure 4.27 Hydrogen bond contribution of the interactions between the β CD molecule and phosphate (green) and glycerol-ester groups (purple) of the lipid and the solvating water molecules (cyan)..... 66
- Figure 4.28 2D-density map on xz -plane of the POPC phosphorus atoms (top) and the β CD molecule (down) for representative BCD3-BCD5 systems, while that of the phosphorus atoms of POPC bilayer alone was given for comparison. The averaged distance between the centers of bilayer and β CD ($r_{\beta CD}$) is also shown.. 67
- Figure 4.29 (Top) local lipid thickness of the POPC membrane bilayer in the systems without and with β CD (no β CD and BCD3-BCD5). (Bottom) 2D-frequency distribution of the β CD molecule in the BCD3-BCD5 systems 68
- Figure 4.30 The β CD in water was independently simulated for 500 ns, and the last MD snapshot is shown in (a). The last snapshots of β CD molecules obtained from the simulations of BCD3 and BCD4 for representing the β CD structure in lipid-water interface and lipid tail region are depicted in (b) and (c), respectively. The primary and secondary rims of β CD molecule are labeled in blue and red, respectively. The backbone atoms of β CD molecules are represented in gray. 70
- Figure 4.31 The average of $r_{\beta CD}$ (black), $r_{P\beta CD}$ (blue) and $r_{S\beta CD}$ (red) for all β CD derivatives in BCD1-BCD5 system 73
- Figure 4.32 The last snapshots of ME β CD simulations 73
- Figure 4.33 The last snapshots of HP β CD simulations 74

CHAPTER 1

INTRODUCTION

Cyclodextrins (CDs) have been widely used in many industrial applications as potent biomolecules by altering physical, chemical and biological properties of guest molecules via their inclusion complex formation. CDs show conformations like truncated cones with a hydrophobic nano-cavity and a hydrophilic outer surface. Because of this special geometry other compounds can be included into the interior of these CDs [1]. The water solubility, stability and bioavailability of ligands are enhanced through CDs complexation. To understand the mechanism of improvement of the properties of CDs-ligand complexes, the formation between the CDs and ligands have been studied both by experiments and theoretical methods. The binding mode and binding affinity between the guest molecule and CDs likely depend on the conformation of CDs and complexed ligands. The various conformations of large ring CDs (LR-CD) are supposed to be excellent host targets even for larger ligands [2, 3]. The formation of more than one cavity influences the ligand loading ability. Thus, the knowledge about CDs conformation is an important to understand their function. Continually, the unbinding process of ligands from CD complexes is also essential, in particular for drug delivery systems (DDS). The drug therapeutic efficiency is subject to not only the water solubility, but also to the membrane permeability of the drug. However, the comprehension of permeation of free CDs, free drugs and CD-drug complexes into the lipid membrane is still unclear.

1.1) Cyclodextrins (CDs)

More than hundred years after CD discovery, CDs are still interesting due to their distinctive properties as seen by an increase in number of publications and patents (Figure 1.1). The studies of cyclodextrins are contributed in various fields such as analytical applications, cell biology, food and cosmetic applications. Especially, the study on CDs in cell biology became highly interesting since a few years (Figure 1.2).

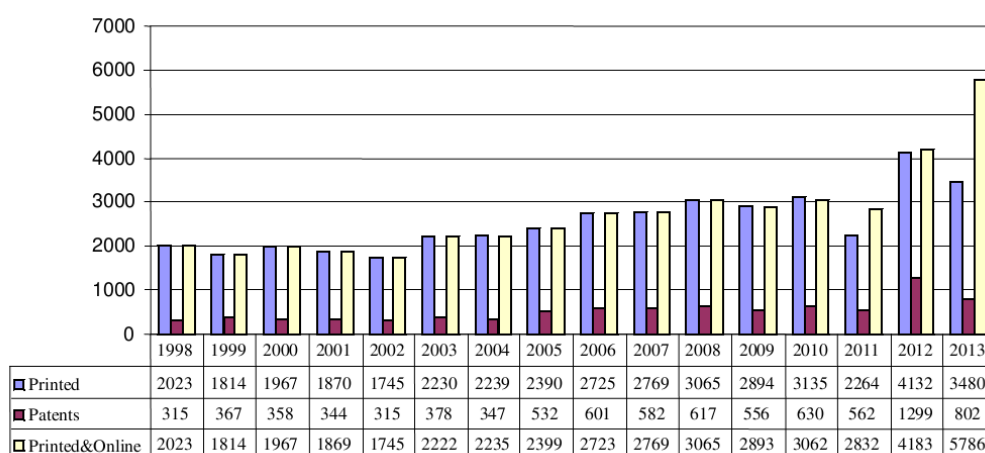


Figure 1.1 Number of publications and patents on cyclodextrin in the past 15 years

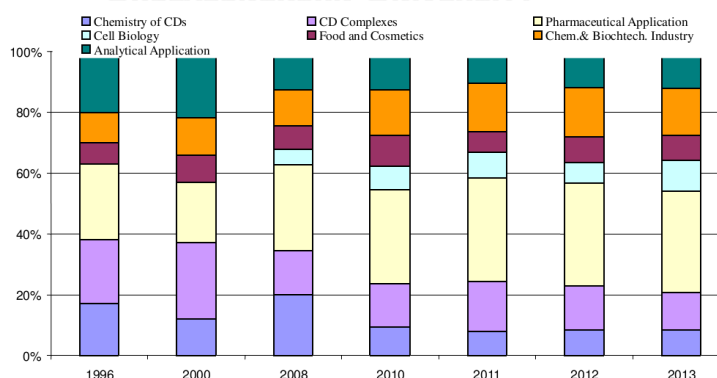


Figure 1.2 Distribution of the publications and patents among the fields of CD applications

CDs are mainly produced by the enzyme cyclodextrin glucanotransferase (CGTases) from starch. They are cyclic α -1,4 linked oligosaccharides of D-glucopyranose units (Figure 1.3). The CDs of various sizes (degree of polymer (DP) up to 100) can be synthesized [4-6]. The most common CDs are composed of six, seven and eight glucose subunits namely as α CD, β CD and γ CD, respectively. These three types of CDs are known as small ring cyclodextrins (SR-CDs). β CD is widely used in food and pharmaceutical industries due to high-yield syntheses and its proper cavity size for small ligand complexation [7]. However, its water solubility is lower than the other SR-CDs. The chemical modification of β CD through substitution of the hydroxyl groups with methoxy groups and 2-hydroxypropyl groups leads to derivatives with significantly higher water solubility about 27 times and 33 times of non-modified β CD, respectively [8]. Moreover, other physicochemical parameters are modified, too. The chemical structures of β CD and its derivatives are represented in Figure 1.3. The majority of CD complexes have a 1:1 [9-13] stoichiometry, but higher order complexes like 2:1 [12, 14] and 2:2 [15] guest–host complexes can occur depending on the relative size of the guest molecule and the CD.

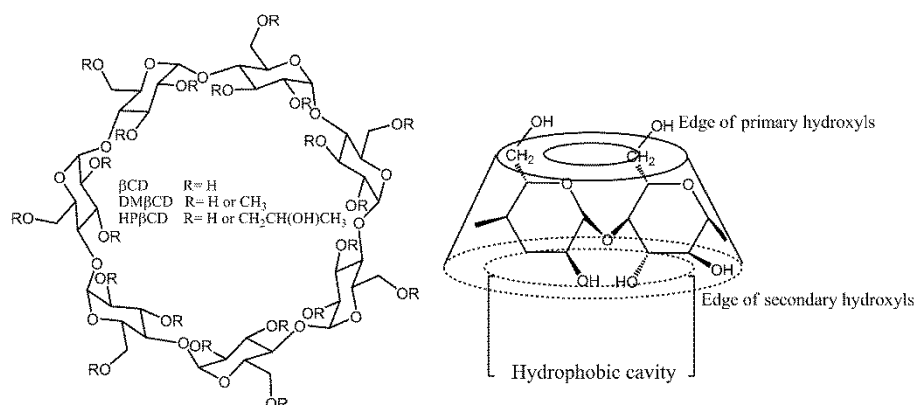


Figure 1.3 (Left) Top and (right) side views of 2D structure of β CD and its derivatives, methylated- β CD and 2-hydroxypropyl- β CD.

The SR-CDs are currently synthesized on industrial scale in tons, and they are widely used as food additives and drug complexing agents. Numerous publications emphasized on the CDs-drug complexation, on their structural properties and on drug activity testing. It was found that CDs generally could enhance drug activity. For example, inclusion complexation with the methylated- β CD showed an enhancement of anticancer drug activity for doxorubicin (DOX), docetaxel (DXL), 5-fluorouracil (5-FU) and cisplatin (CDDP). The IC_{50} of focused drugs were decreased on various cancer cell lines, reported by Gross [16]. The drug activity is improved around 3.1-14.3 folds by complexation with methylated- β CD in comparison to the un-complexed drug. Moreover, the drug intracellular accumulation is also increased by 2-3 times. The authors suggested that the enhancement of drug activity could be divided from the increasing dissolution ability of the dissolved drug in pure water by the direct interaction of the CD-drug complexes at the membrane surface. In addition, this assumption is supported by penetration of CDs into the lipid membrane because of their hydrophilic outer surface, high molecular weight, and very low octanol/water partition

coefficient [17, 18]. Also the phase solubility study of inclusion complexes is a strong evidence of water solubility improvement for several small molecules such as flavonoid compounds [19, 20]. Besides, lipophilic modified CDs (e.g. methylated cyclodextrins) act as penetration enhancer of drug translocation through biological membrane [21]. In drug releasing process, hydrophilic CDs such DM β CD, HP β CD and SB β CD exhibited fast or immediate release pattern. On the other hand, hydrophobic CDs (e.g. ethylated β CD and acylated β CD) serve as prolonged-release drug carriers, as reviewed by Hirayama and Uekama [22].

Although, many research results on host–guest inclusion complexes of regular cyclodextrins including their derivatives are continuously published. The cyclodextrin-lipid interaction related to drug releasing mechanism has been mentioned quite often. Interestingly, CDs are able to extract cholesterol from the membrane. In 2009, the research from Michael S. Brown and Joseph L. Goldstein who received Nobel Prize, also pioneered the study of cholesterol metabolism. They published how CDs assist in moving cholesterol out of lysosomes in Niemann-Pick type C disease [23].

In a theoretical study in 2011, López and co-workers reported the molecular mechanism of dimers of CDs mediated cholesterol extraction by using molecular dynamics simulations. They have been able to study the CD mediated extraction of cholesterol from a pure cholesterol monolayer. The results showed that CDs have a strong affinity to bind to the membrane surface, and, by doing so, destabilize the local packing of cholesterol molecules making their extraction favorable [24]. Continually in 2013, they studied this mechanism with a mixture lipid model and varied the ratio of cholesterol and lipid. They observed that cholesterol could be extracted efficiently upon

adsorption of CD dimers at the membrane/water interface. However, extraction is only observed to occur spontaneously in membranes at high cholesterol levels [25].

Over the last decade, there has been growing interest in the large ring cyclodextrins (LR-CDs) that consist of more than eight glucose subunits. The several sizes of LR-CDs have been achieved by enzymatic syntheses of amyloamylase, another 4α -glucanotransferase which has unique loop structure not existed in CGTase. However, only three crystal structures of ϵ CD (CD10) [26, 27], ι CD (CD14) [27-29] and ϕ CD (CD26) [30, 31] were reported because the high ring flexibility induces the difficulty for crystal formation. LR-CDs can form conformation of various shapes whilst the SR-CDs as CD6, CD7 and CD8 are much more rigid [5, 6, 32]. LR-CDs are originally found in 1965 by French and co-workers [33]. They contain 9-13 glucose subunits, and in 1996 Ueda and co-workers successfully crystallized ϵ CD containing 10 glucose monomers [66] in a bending form. In 1999, CD14 and CD26 were crystallized [27, 31], where CD14 is stable in a bending form like CD10. Interestingly, a twisting configuration containing more than one cavity is found in CD26 [31]. The available X-ray structures of CD10, CD14 and CD26 are depicted in Figure 1.4.

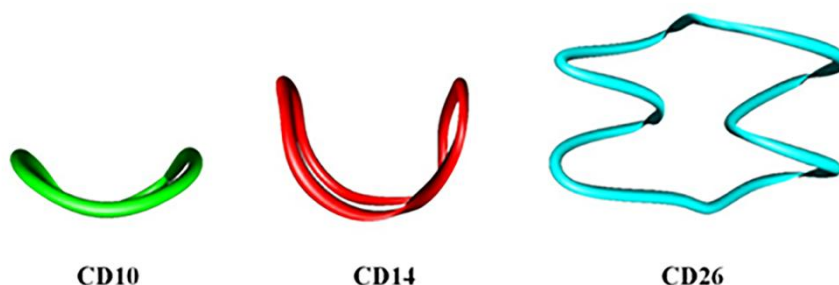


Figure 1.4 Illustration of crystal structures for CD10, CD14 and CD26 [34]

With the polymerization of CGTase, the mixed sizes of CDs are produced. Only LR-CDs with a degree of polymerization of 9-31 were characterized and purified up to now [2]. CDs with a polymerization degree of 22-45 and higher than 50 exhibit an artificial chaperone property for protein refolding [35], they are marketed in Japan as a new product through starch catalysis by amyloamylase for refolding protein kit in 2001. In 2002, Ueda [2] reviewed LR-CD studies on structural and chemical properties of these compounds. An enhancement of water solubility for the LR-CDs was observed. LR-CDs showed also a decrease in half-life of ring opening (Table 1.1). Currently, LR-CDs are commercialized as a chemical by Ezaki Glico Co., Ltd.. The syntheses of LR-CDs are produced by various types of CGTases. The production yield and degree of polymerization of LR-CDs depend on the type of CGTases and reaction conditions. In 2004, Qingsheng Qi and co-workers [36] studied the effect of temperature on transglycosylation reaction by CGTases from *Bacillus macerans* for LR-CDs syntheses. LR-CDs were synthesized at two reaction temperatures of 40 °C and 60 °C. The reaction at 60 °C produced higher LR-CD yield and the obtained yield was about 50% of the total glucan substrate in the reaction. Moreover, the concentration of ethanol in the solution also resulted in an increasing amount of LR-CDs [36, 37].

Table 1.1 Physicochemical properties of LR-CDs compared with those of SR-CDs [2]

	Number of glucopyranose units	Aqueous ^a solubility (g/100 mL)	Surface ^a tension (mN/m)	Specific rotation [α] _D ²⁵	Half-life of ^b ring opening (h)
α -CD	6	14.5	72	+147.8	33
β -CD	7	1.85	73	+161.1	29
γ -CD	8	23.2	73	+175.9	15
δ -CD	9	8.19	73	+187.5	4.2
CD ₁₀	10	2.82	72	+204.9	3.2
CD ₁₁	11	>150	72	+200.8	3.4
CD ₁₂	12	>150	72	+197.3	3.7
CD ₁₃	13	>150	72	+198.1	3.7
CD ₁₄	14	2.30	73	+199.7	3.6
CD ₁₅	15	>120	73	+203.9	2.9
CD ₁₆	16	>120	73	+204.2	2.5
CD ₁₇	17	>120	72	+201.0	2.5
CD ₁₈	18	>100	73	+204.0	3.0
CD ₁₉	19	>100	73	+201.0	3.4
CD ₂₀	20	>100	73	+199.7	3.4
CD ₂₁	21	>100	73	+205.3	3.2

^a Observed at 25 °C.

^b In 1 mol/L HCl at 50 °C.

Nevertheless, the isolation and characterization of LR-CDs with high degree of polymerization are quite difficult. Theoretical studies became another choice to investigate the structural properties at molecular level. The dynamical properties were investigated by molecular dynamics (MD) simulation techniques starting from the crystallized structures (CD₁₀, CD₁₄ and CD₂₆) [34] and larger macro-ring size models (CD₂₇₋₃₀, 35, 40, 48, 55, 70, 85, and 100) including intermediate conformations of available X-ray structures (CD₁₁₋₁₃, CD₁₅₋₁₈, and CD₂₀₋₂₅) in either gas or solution phase [38-46]. Remarkably, the MD results of CDs with a degree of polymerization > 13 supported the hypothesis of the existence of more than one cavity in LR-CDs.

1.2) Biological membrane

The biological membrane, or biomembrane, acts as a selective permeability barrier of molecule transportation between outer and inner moiety of the living cell. The membrane permeability of non-highly charged molecules, small-size molecules and molecule at high concentration such as water is higher than of charged molecules with bulky solvation shell. In common, the biomembrane consists of three major components *i.e* lipids, proteins and carbohydrates. They are formed by non-covalent assemblies, the proteins are embedded in lipid layer and the carbohydrate moieties are always bound at cell exterior (Figure 1.5a). Focusing on lipids, there are three main types of lipids in biomembranes *i.e.* phospholipid, glycolipid and cholesterol. Phospholipids are a major component of cell membranes. They can spontaneously form bilayers, vesicles and micelles in solution because of their amphiphilic characteristic. The phospholipid is composed of *i*) polar group (head) of phosphate *ii*) non-polar (tail) of fatty acid that connected by glycerol. The phosphate group can be modified by organic molecules as choline and alcohols (Figure 1.5b). The macromolecule formation depends on the shape of assembled phospholipids, *e.g.* micelles are formed by the cone phospholipids whereas the phospholipids of the bilayer are cylinders. Besides, the fatty acid chain length and fatty acid chain saturation can be varied. Thus, the characteristic or types of phospholipids depend on their components. The nomenclature of phospholipids is defined by a four-letter code, the first two letters describe the lipid tail and the last two letters the lipid head group (Figure 1.6a). In general, the type of phospholipids and their component ratio in the cell membrane are

different depending on the type of cell membrane (Figure 1.6b). As lipid composition alterations, the PC type is the most contributed in resting mammalian cell [47].

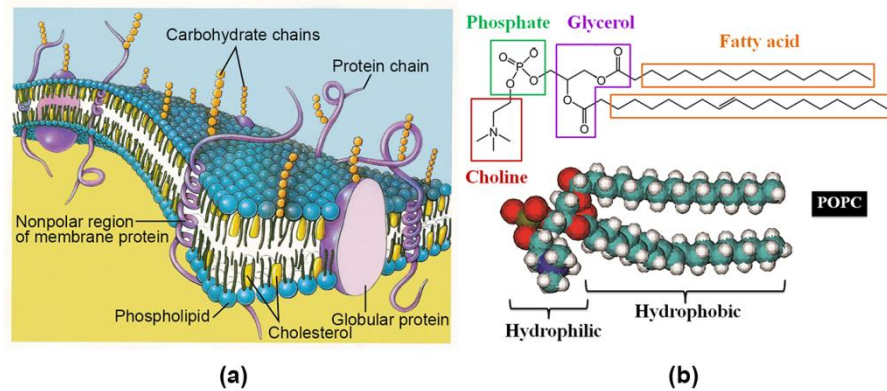


Figure 1.5 (a) Common features of plasma membrane containing three main components as phospholipids, proteins and carbohydrates and (b) The structure pattern of 1-palmitoyl-2-oleoyl-sn-glycero-3-phosphocholine (POPC) phospholipid (modified from https://online.science.psu.edu/biol011_active002/node/4181)

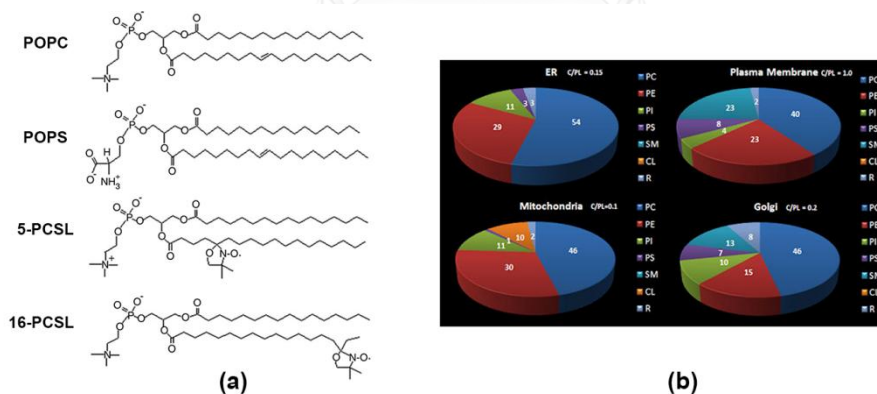


Figure 1.6 (a) Example of phospholipids and (b) Distribution of phospholipids in various parts of mammalian cell [47]

1.3) Molecular dynamics (MD) technique

MD simulation technique plays an important role in the study of complex biological systems. The macroscopic information both on static equilibrium properties

(e.g. binding mode, the averaged molecular structure, the average potential energy of a system) and also on the dynamic properties (such as the viscosity, diffusion coefficient, the dynamics of phase changes) can be achieved [48-50]. The investigation of the structure and dynamics of biological systems of interest leads to a better understanding of their functionality. Based on MD algorithm, the force field or potential energy function is a key of calculation accuracy. The structural and energetic properties of molecules of a system should be validated before starting the simulation. For example, the calculated free enthalpy of solvation of cyclohexane based on GROMOS force field (53A5/53A6 version) exhibited a small absolute mean deviation of only 2 kJ/mol from experimental data [51]. The force field of biomolecules, especially proteins are quite well verified, as implemented in AMBER99 [52], CHARMM27 [53], and GROMOS 53A6 [51, 54]. However, the development of carbohydrate and nucleic acid force fields is still a challenge. Previous studies showed that the MD technique can provide reliable microscopic properties in several complex systems such as proteins, lipids and carbohydrates as well as their combinations. MD simulations have been applied in many studies of cyclodextrin systems as well [55-59]. The binding and unbinding process of guest molecules from CDs complexes can be described this way. The binding pattern and binding efficiency have been investigated by considering structural changes and binding free energy calculations [60-62]. For example, also the enantiomer-selective inclusion mechanism into CDs could be understood [61, 63, 64]. Additionally, the influence of the environment, the solvent on the geometry and the stability of the CD-reaction complexes can be determined [65, 66]. In case of permeation studies of molecules into the cellular membrane, experiments on molecular level are rather difficult. However, even the permeation of quite large molecules such as carbon

nanotubes and fullerene C60 through lipid membranes can be revealed by MD techniques [67, 68]. Besides, the developed classical MD method as replica exchange molecular dynamics (REMD) simulation [69-72] is one of appropriate technique for molecular conformation study. The single classical MD simulation at low temperature condition, which tends to get in a large number of local minima are solved. The advanced method exchanging non-interacting replicas of the system at several temperatures of REMD can overcome the multiple-minima problem leading to an easy approach of global minima. This REMD method has been frequently used for the conformation study of various biomolecules [73, 74].

1.4) Research rational

Regarding to above mentions, computer simulation techniques can provide reasonable results for microscopic properties for complex biological systems. The obtained information is expected to fill the gap between existing theoretical consideration and experimental evidences. As for LR-CD systems, the difficulty in the single crystal preparation and the complexity of the purification process are limitation for conformational studies. Likewise, the permeation mechanism of CDs into lipid membrane is unclear up to now. Additionally, experiments on this topic are difficult to perform, and their results need theoretical support to some extent. Therefore, in the present work, the REMD simulations and the micro-scale MD simulations were used to remedy the problems that are mentioned above by determining the structural and dynamic properties of CDs as well as the interaction of CDs-membrane.

1.5) Research objectives

Hence, this project is divided into two parts and the objectives for each part are mentioned as follows.

Part I: Conformational diversity of cyclodextrins

- To investigate the conformational properties of SR- and LR-CDs by REMDs technique
- To explain the temperature effect to CD conformational change

Part II: Study of permeation mechanism of β cyclodextrin and its derivatives through the biological membrane

- To visualize the penetration mechanism of β cyclodextrin and its derivatives to the biological membrane

The information on structural and dynamic properties including the visualization of CD permeation mechanism could help on the further design of CD-based drug delivery systems and for other applications.

CHAPTER 2

THEORETICAL BACKGROUND

2.1) Molecular Dynamics (MD) simulation

Molecular dynamics (MD) simulation is defined as “computer simulation technique where configuration of concerned atoms or molecules is explored on the basis of the time evolution by integrating their equation of motion” [48-50].

2.1.1) Equation of motion

The Newton’s second law can solve the movement of N interacting atoms:

$$F_i = m_i a_i = m_i \frac{dv_i}{dt} = m_i \frac{dr_i^2}{dt^2}, i = 1, 2, 3, \dots, N, \quad (2.1)$$

where F_i is the force which acts on the atom i , m_i is mass of the atom i and a_i is acceleration of atom i . The acceleration (a_i) can be transformed into the first derivative of velocity (v_i) and the second derivative position (r_i) with respect to the time t .

The forces between concerned atoms are defined by the negative derivatives of potential energy; $V(r_1, r_2, r_3, \dots, r_N)$

$$F_i = -\frac{dV_i}{dr_i} \quad (2.2).$$

By combination of eq. (2.1) and eq. (2.2), Newton’s equation of motion can then relate the derivative of the potential energy to the changes in position as a function of time eq. (2.3).

$$F_i = m_i \frac{dr_i^2}{dt^2} = -\frac{dV_i}{dr_i} \quad (2.3)$$

Solving of equations is conducted simultaneously in small time steps (dt). The coordinates and velocities are updated as a function of time. A simplified description of the standard molecular dynamics simulation algorithm using a predictor-corrector-type integrator is illustrated in Figure 2.1. After initial changes, the system will reach an equilibrium state. The averaging over an equilibrium trajectory can be used to describe many macroscopic properties of the simulation system.

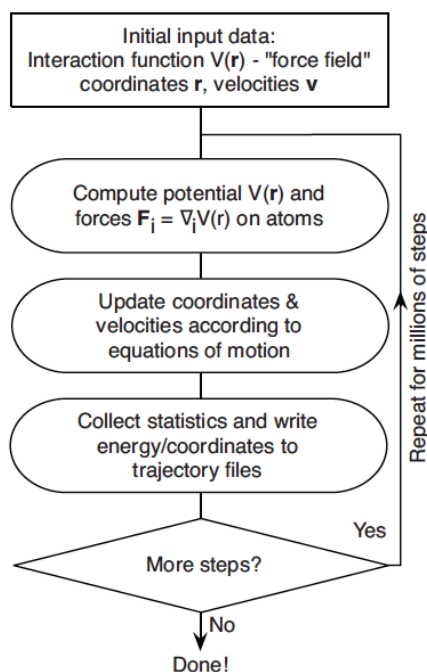


Figure 2.1 A standard molecular dynamics simulation algorithm, e.g. as implemented in GROMACS [49, 75]

The force on atom i at time t is calculated by the potential function (V_{pot}). The details of potential function will be mentioned at below (section 2.1.3). From the Newton's law, the acceleration of the particles can be determined by $a = \frac{F}{m}$, which are then combined with the position and velocities at a time t to calculate the position and

velocities at a time $t + dt$. The force is assumed to be constant during the time step (dt). The forces on the particles in their new positions are then computed, resulting in new positions and velocities at time $t + 2dt$, and so on. To generate the velocities and positions of next atomic movement, the integration is applied on the differential equation of motion. By using the integrator, the initial positions and velocities must be provided. The initial positions of molecules can be extracted from experimental data of X-ray coordinates or can be created from some available molecule builder program. Besides, the initial velocities can be estimated based on the Maxwell-Boltzmann distribution function.

2.1.2) Numerical integration

The differential equation of motion is integrated using finite difference method, several algorithms of which are generally applied in MD simulation. All integrating algorithms assume that the positions, velocities, acceleration, etc. can be approximated by a Taylor expansion.

$$r(t + dt) = r(t) + dtv(t) + \frac{1}{2}dt^2a(t) + \frac{1}{6}dt^3b(t) + \frac{1}{24}dt^4c(t) + \dots \quad (2.4)$$

$$v(t + dt) = v(t) + dta(t) + \frac{1}{2}dt^2b(t) + \frac{1}{6}dt^3c(t) + \dots \quad (2.5)$$

$$a(t + dt) = a(t) + dtb(t) + \frac{1}{2}dt^2c(t) + \dots \quad (2.6)$$

Where v is the velocity (the first derivative of positions with respect to time t), a is acceleration (the second derivative of position with respect to time t), b is the third derivative and c is the fourth derivative.

The Verlet algorithm is most widely used for MD integrator. Based on the Verlet algorithm, the new positions $r(t + dt)$ are estimated by the positions $r(t)$ and the accelerations $a(t)$ at time t and the positions at the previous step $r(t - dt)$.

$$r(t + dt) = r(t) + dtv(t) + \frac{1}{2}dt^2a(t) \quad (2.7)$$

$$r(t - dt) = r(t) - dtv(t) + \frac{1}{2}dt^2a(t) \quad (2.8)$$

The new position $r(t + dt)$ are given by summation of eq. (2.7) and eq. (2.8).

$$r(t + dt) = 2r(t) - r(t - dt) + dt^2a(t) \quad (2.9)$$

From eq. (2.9), the Verlet algorithm uses no explicit velocities, leading in straightforward and modest storage requirements. However, the drawback of the Verlet algorithm is of moderate precision. The numerical error is caused by the combination of small term $dt^2a(t)$ and the large terms $2r(t)$ and $r(t - dt)$. In conclusion, the next positions and velocities at $t + dt$ can be determined by eq. 2.10 and eq. 2.11, respectively, where $a(t) = \frac{F(t)}{m}$.

$$r(t + dt) = r(t) + dtv(t) + \frac{1}{2}dt^2\frac{F(t)}{m} \quad (2.10)$$

$$v(t + dt) = v(t) + dt\frac{F(t)+F(t+dt)}{2m} \quad (2.11)$$

Afterward, the Verlet modified algorithms have been developed. The leap-frog algorithm uses the velocities at $t + \frac{1}{2}dt$ to calculate the position at $t + \frac{1}{2}dt$ as shown below:

$$r(t + dt) = r(t) + dtv(t + \frac{1}{2} dt) \quad (2.12)$$

$$v\left(t + \frac{1}{2} dt\right) = v\left(t - \frac{1}{2} dt\right) + dt \frac{F(t)}{m} \quad (2.13)$$

From eq. (2.12) and eq. (2.13), the velocities leap over the position, and then the position leap over the velocities, like frog jump. By comparing these two algorithms, the leap-frog leads to a better numerical precision than the Velet one. But, the disadvantage is that the velocities and positions are not calculated at the same time. Recently, other integrating algorithms have been used in MD simulations. The Beeman algorithm, which used a more accurate expression for the velocity can give a better energy conservation. But this complex expression requires an expensive computer power. To decide which is the most appropriate integration algorithm to use, the following criteria should be taken into account: the energy conservation, computer power requirement, the permit of long time step integrating, etc.

2.1.3) Potential function

As mention above, the atomic forces can be estimated by the force field or potential functions. Based on molecular mechanics (MM), the potential function (V_{pot}) of a molecule is defined by several terms of atomic motions as described in equations (2.14) and consists of bonded and non-bonded interactions.

$$V_{pot} = V_b + V_\theta + V_\phi + V_{ele} + V_{vdW} \quad (2.14)$$

The different contributions to the total interaction energy are shown in Figure 2.2 [76, 77]. The energy terms related to covalent bonds are the bond energy V_b , the bond angle energy V_θ and the dihedral angle energy V_ϕ . The last two terms are non-

bonded interactions, electrostatic V_{ele} and van der Waals V_{vdW} interactions. The potential energy of the system could, in principle, be solved from the electronic structure of the atoms [78, 79], However, in the case of complex molecular systems this is not easy possible for the moment, as these methods need very large computer resources. Instead, the potential energy is calculated only as a function of nuclear positions, as described here.

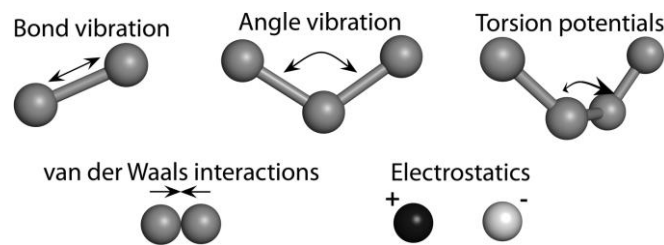


Figure 2.2 Typical molecular mechanics interactions used in GROMACS

The bonds and angles are the first approximation typically described as harmonic oscillators. Therefore, the bond energy (V_b) is

$$V_b = \sum \frac{1}{2} k_b (r_{ij} - r_{ij}^0)^2, \quad (2.15)$$

where r_{ij} is the distance between atom i and j , r_{ij}^0 are the equilibrium values of bond distance and k_b is force constants for a particular bond.

And, the bond angle energy (V_θ) is given by

$$V_\theta = \sum \frac{1}{2} k_\theta (\theta_{ijk} - \theta_{ijk}^0)^2, \quad (2.16)$$

where θ_{ijk} is the angle between atom i , j and k , θ_{ijk}^0 are the equilibrium values of valence angle and k_θ is the force constant for valence angles.

The dihedral angle energy (V_ϕ) is presented as the sum of cosine expansion as presented in eq. (2.17).

$$V_\phi = \sum \frac{1}{2} k_\phi (1 + \cos(n\phi - \phi^0)) \quad (2.17)$$

The ϕ is the value of the dihedral angle, ϕ^0 is the equilibrium value of dihedral angle, k_ϕ is the force constant affecting the barrier height and n the multiplicity giving the number of minimum points in the function as the bond is rotated through 360° .

As for the non-bonded interactions, the electrostatic interaction (V_{ele}) is described by the Coulombic term:

$$V_{ele} = \sum \frac{q_i q_j}{4\pi\epsilon_0 r_{ij}}, \quad (2.18)$$

where q_i and q_j are the partial charges of the atoms i and j , r_{ij} is the distance between atom i and j , and ϵ_0 is dielectric constant. The van der Waals interaction term describes the repulsion and the dispersion between the atoms and is often approximated by the Lennard-Jones formula:

$$V_{vdW} = \sum \left(\frac{A_{ij}}{r_{ij}^{12}} - \frac{B_{ij}}{r_{ij}^6} \right) \quad (2.19)$$

where A_{ij} and B_{ij} are the coefficients for repulsion and dispersion, respectively.

2.2) Temperature Replica Exchange Molecular Dynamics (T-REMD)

It is known that biomolecules have many local-minimum free energy states. By classical MD, it is difficult to process the global minimum because the molecule could be trapped in a local minimum. The replica exchange molecular dynamics (REMD) was

developed to solve this classical MD limitation in conformation searching. The concept is that REMD runs multiple isothermal MD simulations in parallel at a sequence of increasing of temperatures ($T_1, T_2, T_3, \dots, T_n$) and periodically efforts to exchange between temperatures (Figure 2.3).

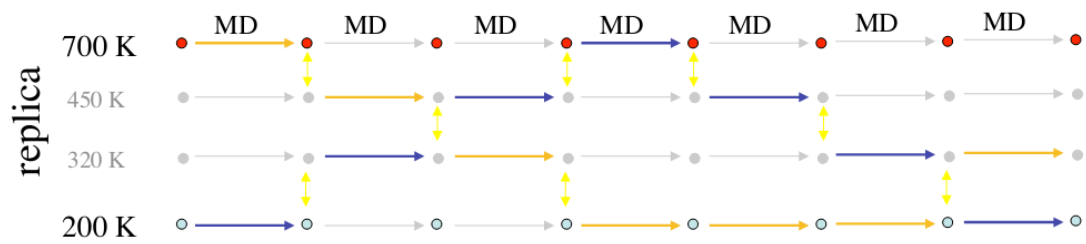


Figure 2.3 The ideal of temperature replica exchange MD simulation

REMD allows the simulation exchange between state X (replica i with T_1 and replica j with T_2) and state X' (replica i with T_2 and replica j with T_1) with the transition probability $w(X \rightarrow X')$ according to the Metropolis algorithm given below.

$$w(X \rightarrow X') = \begin{cases} 1, & \text{for } \Delta \leq 0 \\ \exp(-\Delta), & \text{for } \Delta > 0 \end{cases} \quad (2.20)$$

where $\Delta \equiv (\beta_1 - \beta_2)(V(x_j) - V(x_i))$, $\beta_1 = \frac{1}{k_B T_1}$ and $\beta_2 = \frac{1}{k_B T_2}$

REMD makes random walks in the temperature space, and efficient sampling is realized in the conformational space without getting trapped in local-minima state. The distributions of dihedral angles (Φ, ψ) of Gly-2 of Met-Enkephalin in gas phase at temperature 200 K from the classical MD and replica exchange MD are compared in Figure 2.4.

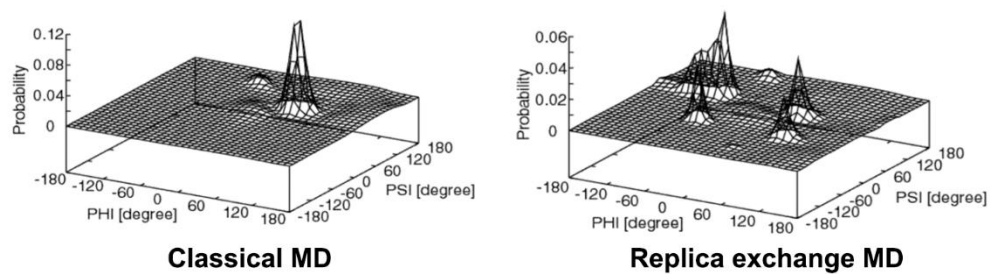


Figure 2.4 Comparison between the structural analysis of classical MD and replica exchange MD [70]



CHAPTER 3

METHODOLOGY

In order to understand the molecular details of the CD conformations and the interaction between CDs and the lipids of the biological membrane, the computer simulation techniques as the replica exchange MD and classical MD were applied for research in part I and part II, respectively. The project overview is presented in Figure 3.1. The details of the study process in each part are separately mentioned as shown below.

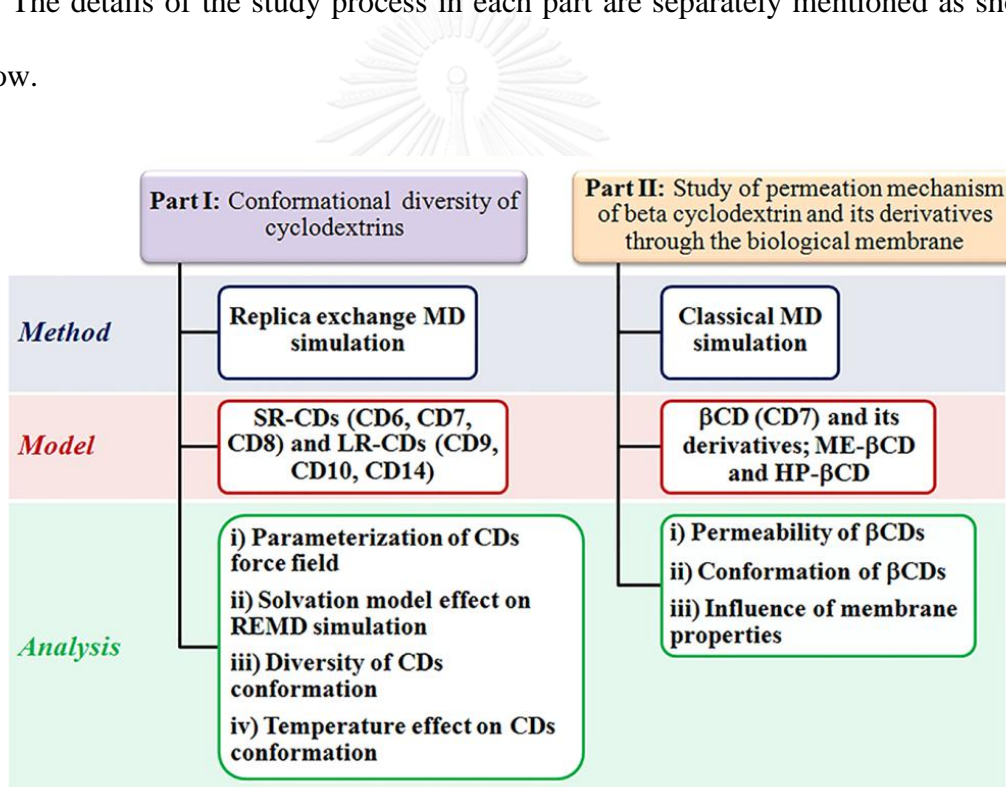


Figure 3.1 Overview of research project

3.1) Part I: Conformational diversity of cyclodextrins

The study focused on the conformational diversity of CDs both for SR-CDs and LR-CDs. All CDs structures CD6, CD7, CD8, CD10 and CD14 were taken from the

Cambridge Crystallographic Data Center (CCDC) entry code BANXUJ [32], BUVSEQ02 [5], CIWMIE10 [6], CCDC100656 [80] and CCDC124917 [80], respectively. The X-ray structure of the hydrated CD9 was reported to be of bent shape, however, the coordinates are not available [81]. Thus, the bent form of CD9 was modified from the X-ray structure of CD10. All structure preparations and REMD simulations were performed by AMBER10 program. The testing of the force field and the effect of the Generalized Born (GB) solvent model was conducted by the representative REMD simulation of CD10. Several carbohydrate force fields as Glycam04 [82-84], Glycam06 [85-88] and hybrid force field q4md-CD [89] were considered. The GB implicit solvent model was varied as Igb1, Igb2 and Igb5 [90]. The CDs starting structures were fully minimized with 2000 steps of steepest descent (SD) method, followed by 1000 steps of conjugated gradient (CG) method to reduce unfavorable steric interactions. To obtain reasonable REMD simulation results, which have suitable potential energy overlapping between each replica and nearby, the REMD conditions, *i.e.*, temperature range and interval as well as number of replica were firstly taken into account. These conditions were tested on the REMD simulation of CD10, testing of force field and GB solvent model. Here, all REMD simulations of CDs were performed with 16 replicas at temperatures ranging from 300 K to 600 K with interval steps of 20 K. To equilibrate the systems at the assigned temperatures, a short MD simulation of 5 ns was performed prior to the REMD simulation. The REMD simulation was then done for 100 ns using Glycam06 force field and the solvent model Igb5. The REMD simulations allowed exchanging structures every 4 ps where the number of exchange steps is 25000.

The conformational change of CDs was monitored through contour plots of the probabilities of the distances between the secondary hydroxyl groups of adjacent glucoses, $d_1[\text{O2}_{(n)}\text{-O3}_{(n+1)}]$, and the distances between the glycosidic oxygen atoms, $d_2[\text{O4}_{(n)}\text{-O4}_{(n+1)}]$. Other structural properties such as $d_3[\text{O2-O6}']$, $d_4[\text{O3-O6}']$, $d_5[\text{O3-O5}']$, $\theta[\text{C6-C2}'\text{-C6}']$ and $\tau[\text{O2-C1-C4}'\text{-O3}']$ were also calculated referring to the flip character of each glucose subunit on CD's ring. The shape of macro-ring was investigated by bending, ring circularity and radial of gyration. All measurement of distances, angle, hydrogen bonding and radial of gyration were performed by the ptraj module in AMBER10 package. In this study, we opposed the two new molecular-structure analytical methods, which are biplanar angle and circularity. The analysis codes were implemented in Python 2.7 utilizing scikit-learn machine-learning toolkit version 0.15.0 for data analysis, scipy version 0.14.0 and numpy version 1.8.1 for numerical and mathematical supporting subroutines. According to these structural property calculations, the possible CD conformations could be identified as well as the temperature effect on their structures. Moreover, the exchange energies of CD structures were estimated based on Maxwell–Boltzmann statistics.

3.2) Part II: Study of permeation mechanism of beta cyclodextrin and its derivatives through the biological membrane

In this part, we focused on the permeability of β CD and its derivatives as ME β CD and HP β CD on lipid bilayer of 1-palmitoyl-2-oleoyl-sn-glycero-3-phosphocholine (POPC), a common component of eukaryotic cell membranes. The system preparations and MD simulations for all focused models are performed by using GROMACS package version 4.5.5 [49]. The optimized β CD based on quantum

chemical calculations was used as initial structure [91]. In the case of the ME β CD and HP β CD derivatives, hydroxyl groups on all glucose subunits at 2- or 6- or 2, 6-position of β CD were substituted by methyl groups and 2-hydroxypropyl groups, respectively. The starting coordinates of 128 POPC bilayer units were taken from Tieleman's group (<http://wcm.ucalgary.ca/tieleman/downloads/popc128b.pdb>). The details of seven focused β CD models with different substituent groups and substituted positions are summarized in Table 3.1.

Table 3.1 Details of focused β CD models

No.	system	2-position	3-position	6-position
1	β CD	-OH	-OH	-OH
Methyl substitution				
2	2-ME β CD	-OCH ₃	-OH	-OH
3	6-ME β CD	-OH	-OH	-OCH ₃
4	2,6-DM β CD	-OCH ₃	-OH	-OCH ₃
Hydroxypropyl substitution				
5	2-HP β CD	-OCH ₂ CH(OH)CH ₃	-OH	-OH
6	6-HP β CD	-OH	-OH	-OCH ₂ CH(OH)CH ₃
7	2,6-HP β CD	-OCH ₂ CH(OH)CH ₃	-OH	-OCH ₂ CH(OH)CH ₃

At the beginning, the interactions between β CD and POPC bilayer were taken into account. Five initial configurations of β CD have been varied with the different molecular orientations and locations, as defined in the BCD1-BCD5 systems, shown in Figure 3.2a-e. In BCD1-BCD3 systems, the β CD molecule was initially located in the water phase at a distance of 3.5 nm in z direction from the center of bilayer. Meanwhile the BCD4 and BCD5 systems represented geometries where the β CD molecule was placed initially at the center of lipid bilayer. These setups allow us to study the behavior

of β CD in bilayer, and this technique has been widely used in the simulations of molecular transportation into membranes [4, 92, 93]. The same pattern of initial model setups was applied for the other assigned β CD derivatives. All simulations were prepared and performed by GROMACS package version 4.5.5 [49]. The β CD molecule was described by the carbohydrate force field in GROMOS 45A4 [24, 94], and POPC molecule was performed with the modified Berger *et al.* parameters [95, 96]. The POPC lipid bilayers were fully solvated by 7122 molecules of single point charge (SPC) water [97] in the simulation box size of $6.42 \times 6.45 \times 9.19 \text{ nm}^3$.

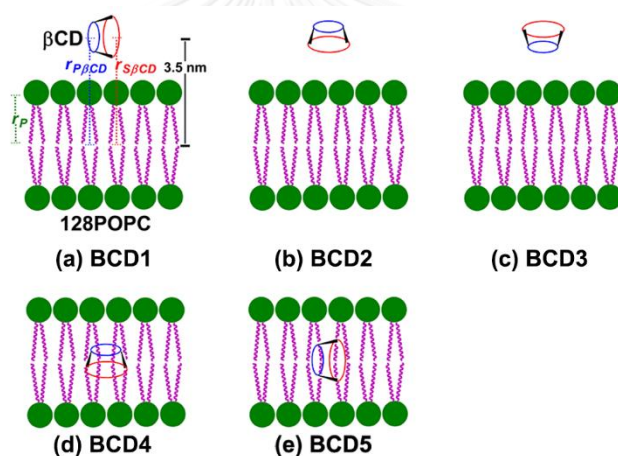
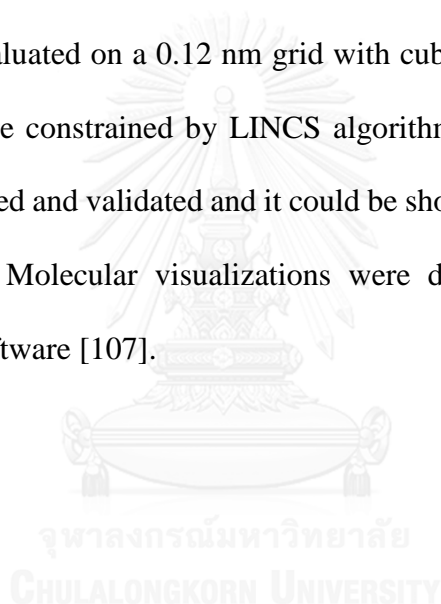


Figure 3.2 (a)-(c): Starting geometries of various orientations β CD at the membrane surface (d)-(e): Starting geometries of various orientations β CD inside the membrane

After the energy minimization with the steepest descent algorithm for 10000 steps, the classical MD simulation was carried out with NPT ensemble (particle number, pressure, and temperature kept constant) at microsecond scale. At least 500 ns equilibrated trajectories were used for further analysis. The integration time step was set at 2 fs and the trajectories were saved every 2 ps. The periodic boundary was applied

in all directions. The β CD, lipid and water molecules were separately thermostated at 298 K by the Parrinello-Bussi velocity rescale algorithm [98, 99]. Semi-isotropic pressure was applied by Berendsen algorithm [100], at an equilibrium pressure of 1 bar both in the xy plane and in the z-direction (bilayer normal) with a time constant of 3.0 ps and a compressibility of $4.5 \times 10^{-5} \text{ bar}^{-1}$. The Lennard-Jones and the real-space parts of electrostatic interactions were cut off at 1.0 nm. The particle mesh Ewald (PME) method [101-103] was used to compute long-range interactions with the reciprocal-space interactions evaluated on a 0.12 nm grid with cubic interpolation of order four. All bond lengths were constrained by LINCS algorithm [104]. The used simulation protocol has been tested and validated and it could be shown that it works well for lipid systems [105, 106]. Molecular visualizations were done using Visual Molecular Dynamics (VMD) software [107].



CHAPTER 4

RESULTS AND DISCUSSIONS

4.1) Part I: Conformational diversity of cyclodextrins

In this part, the conformational diversity of both SR-CDs and LR-CDs is investigated. The conformation diversity of LR-CDs is our main focus because this comprehension was unclear up to now even it is quite well known that the SR-CDs structures should be of cyclic form with one cavity. The study starts with investigation on the conformations of CD10, which is the smallest size of LR-CDs. All REMD setups were trialed on this CD10 model. Then, REMD simulations of all focused CD sizes were performed under those validated REMD conditions. Therefore, the results and discussions are separated into 3 sections *i.e.* 4.1.1) *Validation of REMD simulation setup*; the testing of force field, GB solvate model as well as REMD conditions are considered. After suitable REMD setups have been obtained, independent simulations on each CD ring sizes were performed. Thus, the conformation study of each CD size is separately reported and discussed as follows: 4.1.2) *The conformation change of CD10*; the possible structures of CD10 were investigated based on their flip character. And the last section, 4.1.3) *The conformation change of CD14*; the structures of the larger size of the CD14 were described by new conformation analysis methods as biplanar angle and ring circularity.

4.1.1) *Validation of REMD simulation setup*

To obtain reliable REMD simulations, the validation of simulation setups was conducted on the representative CD10 model. The bent form of the CD10 X-ray

structure is illustrated in Figure 4.1. Firstly, the temperature distribution and number of replica were tested. The calculated overall acceptance ratios of three various solvent models Igb1, Igb2, and Igb5 are 0.51 (the ratio must be greater than 0.1). There is no significant effect of implicit GB solvent model to the distribution of potential energy as shown in Figure 4.2. It can be seen that the temperature range from 300 K to 600 K with 20 K interval is suitable for the CD10 system. Consequently, these REMD conditions are assumed to be used properly in other CD sizes as well.

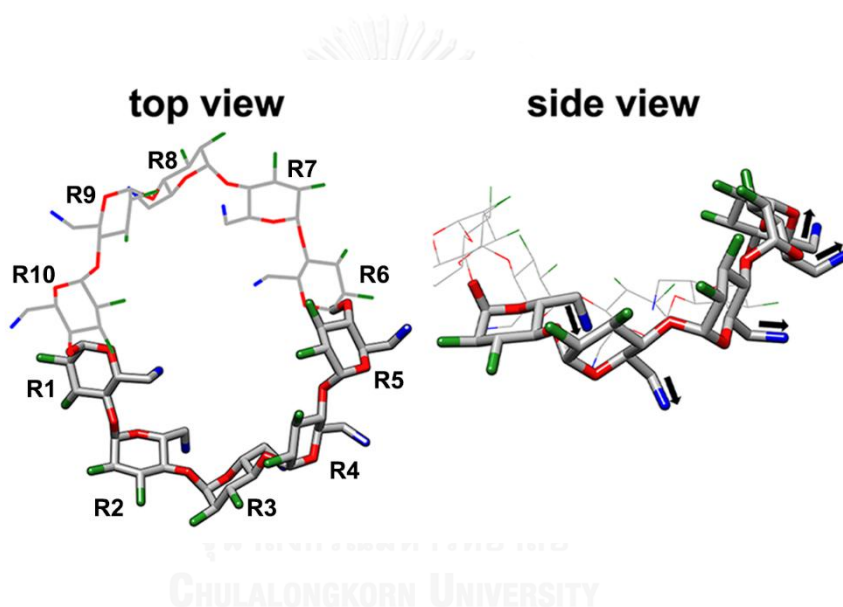


Figure 4.1 Top- and side-view of CD10 X-ray structure, a helical band subunit is shown with five glucose rings as presented in bold sticks.

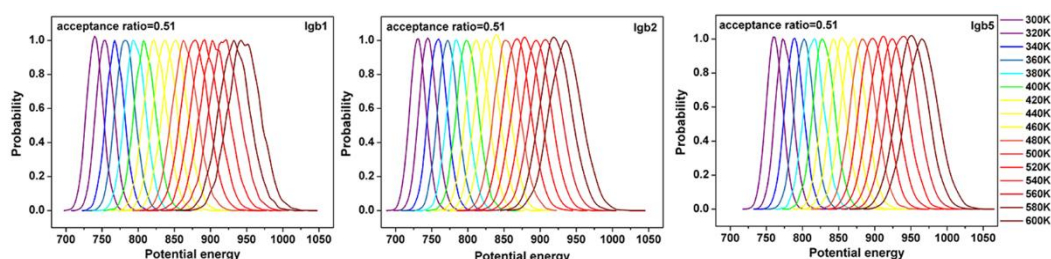


Figure 4.2 The probability distributions of the total potential energy for the REMD simulations with the three solvation models Igb1, Igb2 and Igb5

To investigate the conformational changes of CD10, the distances between the secondary hydroxyl groups of adjacent glucoses, $d_1[\text{O}2_{(n)}-\text{O}3_{(n+1)}]$, and the distances between the adjacent glycosidic oxygen atoms, $d_2[\text{O}4_{(n)}-\text{O}4_{(n+1)}]$, which is less sensitive on the glucose ring flips, but describes the ellipticity of the rim, are plotted for all the snapshots taken from the simulation at 300 K. The definitions of focused parameters are shown in Figure 4.3.

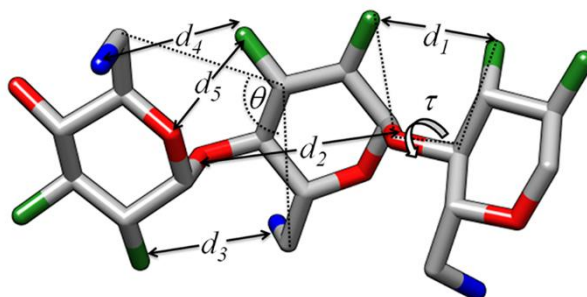


Figure 4.3 (a) CD fragment showing the atomic labels and focused structural parameters, $d_1[\text{O}2-\text{O}3']$, $d_2[\text{O}4-\text{O}4']$, $d_3[\text{O}2-\text{O}6']$, $d_4[\text{O}3-\text{O}6']$, $d_5[\text{O}3-\text{O}5']$ and $\tau[\text{O}2-\text{C}1-\text{C}4'-\text{O}3']$. A turn between two glucose units is shown for the left glucose unit, whereas the two other glucose rings are within the band structure in *cis* position.

The contour lines from the diagrams describe the probabilities for the distance values. Highest probabilities are according to the deepest color (red to blue). In the probability diagrams (Figure 4.4) an accumulation of the distance pairs around (3.5 Å, 4.5 Å) could be found which correlates well with glucopyranose ring connections of the crystal structure, where the 2- and 3-hydroxy groups remain in *cis* position together (at the same side of the rim). The second, less populated accumulation point appears at (5.5 Å, 4.5 Å). These distances are correlated with the turn of the glucopyranose rings

from the *cis* arrangement to a *trans* position of the six-membered rings. Due to the mobility of the ring systems some spreads of the distance values can be observed.

Three different carbohydrate force fields were compared. Their contour plots of the probability distributions are depicted in Figure 4.4. In the case of glycam04 the distances for the *cis* arrangement of the glucopyranose ring systems seem to dominate, only a small population for flip distances can be observed. In contrary, the more reliable glycam06 force field describes conformations with turns of the glucose units. Also, the q4md-CD force field, which has been postulated to give a comparable good description of cyclodextrin geometries, delivers quite similar results as the glycam06 force field (Figure 4.4). In the following the glycam06 force field was applied for all REMD simulations.

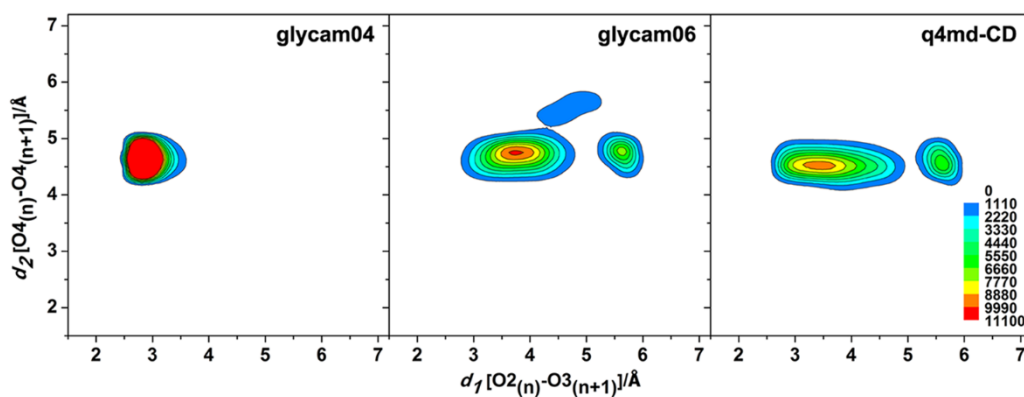


Figure 4.4 Contour plots of the probability distribution of overall snapshots of CD10 with the three different force fields (glycam04, glycam06 and q4md-CD force fields)

Moreover, the effect of GB solvent model on CD10 structural properties was also studied. 50-ns REMD simulations at 300 K in connection with different implicit solvent models (Igb1, Igb2, and Igb5) were conducted and compared with each other

(Figure 4.5). Their 2D probability contours at all assigned temperatures (300-600 K) were plotted in Figures 4.6-4.8.

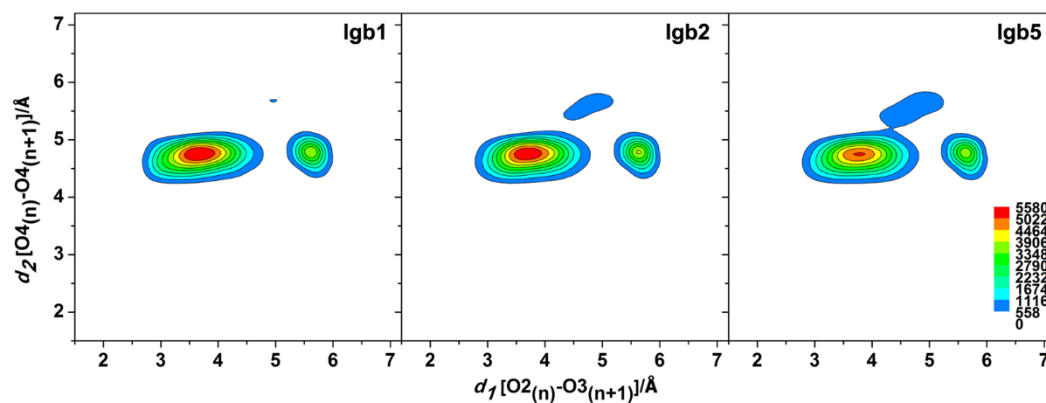


Figure 4.5 Contour plots of the probability distribution of overall snapshots of CD10 with the three different solvation models, lgb1, lgb2, and lgb5 at 300 K

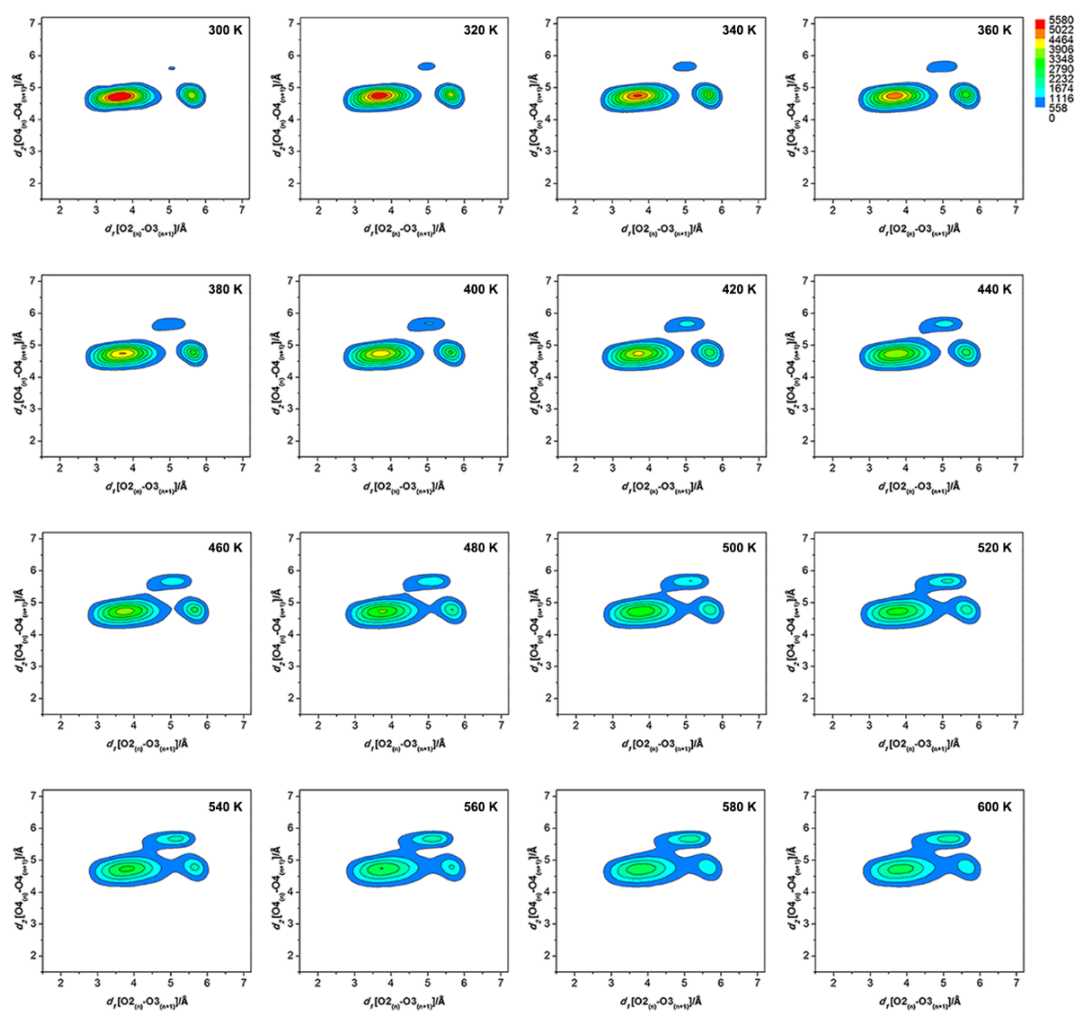


Figure 4.6 The Igb1 contour plots of the probability distribution from the 50-ns REMD simulations of CD10 at temperatures 300-600 K

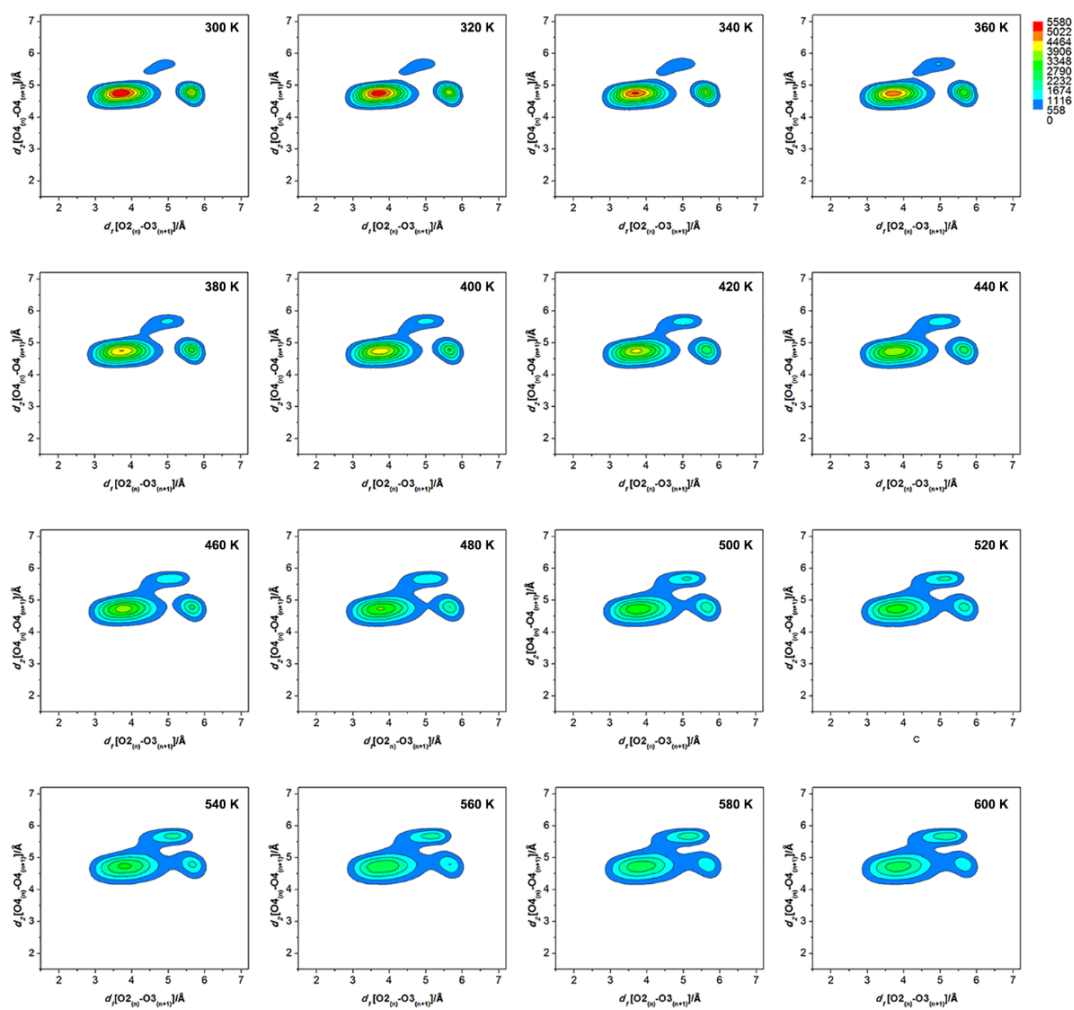


Figure 4.7 The Igb2 contour plots of the probability distribution from the 50-ns REMD simulations of CD10 at temperatures 300-600 K

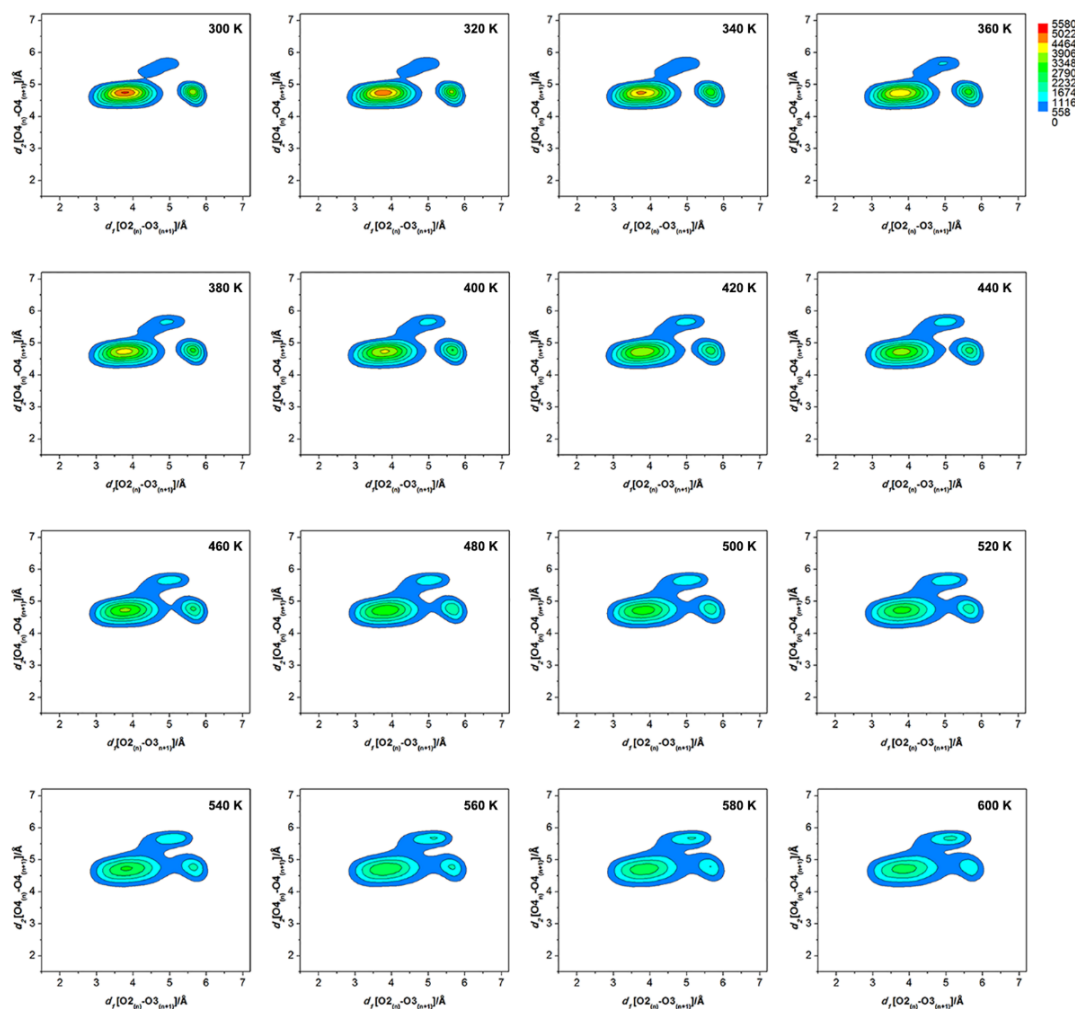


Figure 4.8 The Igb5 contour plots of the probability distribution from the 50-ns REMD simulations of CD10 at temperatures 300-600 K

The results of 50 ns REMD simulations showed that all three probability contours are similar at same temperature, for example at 300 K as seen in Figure 4.5. There are three distinguished major possibilities for ($d_1[\text{O}2_{(n)}-\text{O}3_{(n+1)}]$, $d_2[\text{O}4_{(n)}-\text{O}4_{(n+1)}]$) observed around (3.5 Å, 4.5 Å), (5.5 Å, 4.5 Å) and (5.0 Å, 5.5 Å). These locations take place almost at the same positions although different solvent models are used. The ranking of probability levels is (3.5 Å, 4.5 Å) > (5.5 Å, 4.5 Å) > (5.0 Å, 5.5 Å) at low temperatures, 300-460 K in Igb5, 300-520 K in Igb1 and 300-500 K in Igb2.

The probability contours of (5.0 Å, 5.5 Å) were increased to be equal to that of (5.5 Å, 4.5 Å) when the temperatures are higher than the mentioned temperature ranges. At high temperatures, the probability contours were considerably expanded indicating more flexibility of CD10 conformations. Therefore, the GB solvent model Igb5 can be used as a representative model for the CD conformational study. Then, these validated REMD setups were applied to others CD sizes for both the larger ring of CD14 and the smaller ones CD6, CD7, CD8 and CD9. The 2D contours of probability distribution between $d_1[O2_{(n)}-O3_{(n+1)}]$ and $d_2[O4_{(n)}-O4_{(n+1)}]$ of REMD simulations at 300 K for all focused CDs are compared in Figure 4.9.

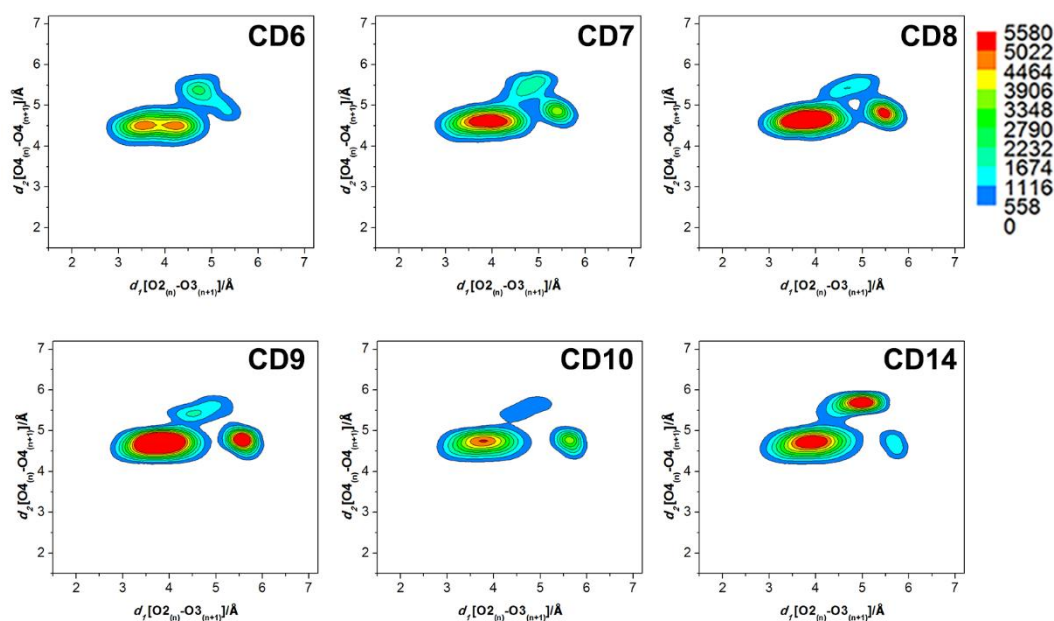


Figure 4.9 Contour plots of the probability distribution of CD6-CD10 and CD14 REMD simulations at 300 K

Figure 4.9 shows that almost all CD simulations gave the rather similar 2D contours, except for CD6. Three main probabilities of ($d_1[O2_{(n)}-O3_{(n+1)}]$, $d_2[O4_{(n)}-$

O_{4(n+1)}]) were observed without significant difference from the simulation of the representative CD10. The highest probability was located at (3.5 Å, 4.5 Å) for all CD sizes. The order of the probabilities of the three locations was (3.5 Å, 4.5 Å) > (5.5 Å, 4.5 Å) > (5.0 Å, 5.5 Å) for the simulations of CD7, CD8, CD9 and CD10. The probability of (5.0 Å, 5.5 Å) increased to higher order than the probability of (5.5 Å, 4.5 Å) for CD14. The size of the smallest ring CD6 is totally different from the other sizes. The area of (5.0 Å, 5.5 Å) disappeared resulting in only two remaining areas were presented. This supports that CD6 is less flexible because it is difficult to form a *trans*-position of the glucose subunits.

From this section, it could be indicate that *i*) REMD simulation could describe the conformational changes of all CDs *ii*) the 16 replicas of REMD simulated at 300-600 K, 20 K interval, can be successfully used for CDs conformational studies, *iii*) the glycam06 force field is reliable for describing the flip of glucose subunits of CDs, *iv*) there is no significant effect of the implicit GB solvent model on CD conformation changes. Therefore, the Igb5 solvent model was chosen as representative for CD conformation studies. Subsequently, REMD simulations based on glycam06 force field and Igb5 solvent model at 300-600 K were extended from 50 ns to 100 ns. Then, all possible CD conformations were described by their structural properties.

4.1.2) *The conformation change of CD10*

The conformation of CD10 was analyzed in terms of the flip or turn character of the glucose subunits within the macrocyclic ring. However, the basic structural properties of CD10 in the crystalline state are quite well understood. Some structural data of the crystal structure are depicted in Table 4.1. The distances of the second half

of the CD ring are identical as a consequence of the C2 symmetry in the crystal. The distance R5-R6 (as well as R10-R1) is much larger because of the flip of the glucopyranose ring.

Table 4.1 The focused structural properties, d_1 [O2-O3'], d_2 [O4-O4'], d_3 [O2-O6'], d_4 [O3-O6'], d_5 [O3-O5'] and τ [O2-C1-C4'-O3'] measured from the crystal structure of CD10 [80].

Ring connecting	$d_1/\text{\AA}$	$d_2/\text{\AA}$	$d_3/\text{\AA}$	$d_4/\text{\AA}$	$d_5/\text{\AA}$	τ/degree
R1-R2	2.89	4.60	6.39	7.35	4.47	-38.1
R2-R3	3.03	4.46	6.01	7.07	4.42	-39.1
R3-R4	2.88	4.36	5.79	7.62	4.82	-12.9
R4-R5	3.91	4.48	6.05	6.80	3.97	-75.2
R5-R6	5.53	4.47	3.93	4.79	3.20	143.4

The dynamical behavior of CD10 in aqueous solution was investigated by REMD simulation and a ranking of the obtained conformations was performed. Thus, the distances of adjacent glucopyranose units d_1 [O2-O3'], d_2 [O4-O4'], d_3 [O2-O6'], d_4 [O3-O6'] and d_5 [O3-O5'] as well as the two angles θ [C6-C2'-C6'] and τ (O2_(n)-C1_(n)-C4_(n+1)-O3_(n+1)) were computed and the results are summarized in Table 4.2. As already mentioned, the definitions of all parameters are presented in Figure 4.3.

The REMD technique is able to describe the effect of higher temperatures during the simulation. In Figure 4.10, the contour plots for 100 ns REMD simulations at 300 K, 400 K, 500 K and 600 K are compared. No principal change of the pattern can be observed, but the spread of the distance distribution increases. This is not unexpected, as higher temperatures will effectuate higher amplitudes of the motion of

the molecule. No additional conformation can be detected, except for a less pronounced accumulation point at (5.0 Å, 5.0 Å).

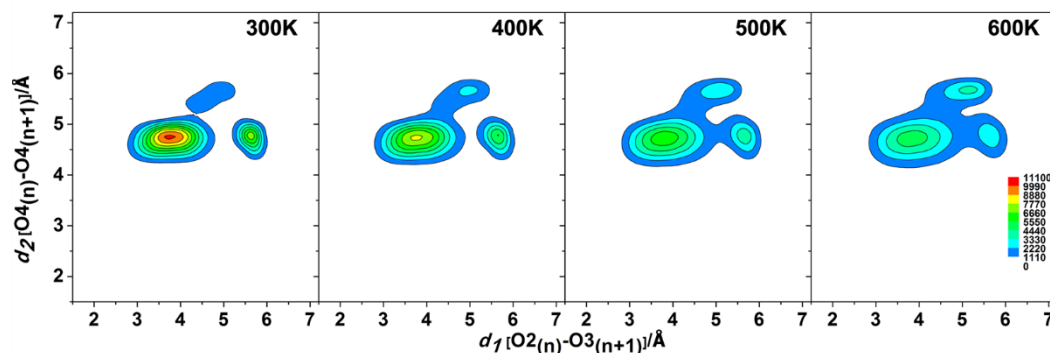


Figure 4.10 Contour plots of the probability distribution of overall snap-shots of CD10 at various temperatures using Igb5 solvent model and glycam06 force field

The conformational changes of CD10 in aqueous solution are determined by several processes. First of all, the ring formed by the O4 oxygen atoms is not planar and there are changes of the geometry of this larger ring system. Second, the occurring movements of the glucose units against each other, including sudden turns leading to a *trans* arrangement can be also seen in the X-ray crystal structure. Another mode of motion is the conformational change of the glucose units itself, and at least the formation and the breaking of intramolecular hydrogen bonds followed by rotations of the hydroxyl groups and the carbon-carbon bond attached to the primary hydroxyl group. These movements are partly concerted and coupled to a high extent. In particular, the turns of the glucose units are thoroughly correlated with the conformational changes of the large ring system.

In order to estimate the number of turns in various conformations, structural parameters have been sampled for 100000 snapshots. The glucose subunit is defined to

turn when the $\theta[C6-C2'-C6']$ (defined in Figure 4.3) is larger than 60 degrees. Some selected values are shown in Table 4.2. The snapshots for each type of conformation have been selected randomly. The angle $\theta[C6-C2'-C6']$ proved to be the most sensitive as well as the most significant parameter for the findings of turns. Values around 90 degrees indicate clearly a turn position of a glucose in the large ring system. Finally, the analysis of the sampled snapshots according to these parameters shows a variety of conformations with different numbers of turns in the macrocyclic ring.



Table 4.2 Structure properties of classified CD10 conformations as considering the number of turns angle (θ), the d_1 [O2-O3'], d_2 [O4-O4'], θ [C6-C2'-C6'] and τ [O2-C1-C4'-O3'] of each connecting unit are compared with X-ray.

	R1-R2	R2-R3	R3-R4	R4-R5	R5-R6	R6-R7	R7-R8	R8-R9	R9-R10	R10-R11
d_1 [O2-O3']										
X-ray	2.89	3.03	2.88	3.91	5.53	2.89	3.03	2.88	3.91	5.53
1-turn	3.90	3.85	3.67	4.85	5.52	3.70	3.65	3.38	3.54	4.77
2-turn(1-5)	4.00	3.56	5.68	4.03	2.75	3.53	3.91	5.68	3.50	3.30
2-turn(1-4)	4.05	4.54	3.87	5.40	4.38	3.89	5.12	5.55	2.94	3.13
3-turn	4.16	4.34	4.71	5.78	3.54	3.93	4.18	4.82	5.85	3.29
4-turn	4.60	4.85	4.83	3.90	3.12	3.77	4.42	5.88	4.65	3.89
d_2 [O4-O4']										
X-ray	4.60	4.46	4.36	4.48	4.47	4.60	4.46	4.36	4.48	4.47
1-turn	4.95	4.61	4.49	5.66	4.43	4.51	4.54	4.66	4.80	5.55
2-turn(1-5)	4.90	4.32	4.93	4.81	4.69	4.78	4.45	4.73	4.65	4.47
2-turn(1-4)	5.00	5.39	4.72	5.54	4.56	4.62	4.73	4.59	4.55	4.67
3-turn	4.42	4.52	5.60	4.76	4.63	4.58	4.57	5.44	4.55	4.58
4-turn	5.51	5.51	5.69	4.42	4.25	4.32	5.61	5.04	5.26	4.54
θ [C6-C2'-C6']										
X-ray	33.0	32.4	26.6	38.7	88.0	33.0	32.4	26.6	38.7	88.0
1-turn	35.9	29.3	35.0	38.1	86.1	32.7	33.0	30.6	45.2	50.9
2-turn(1-5)	30.5	29.7	85.7	32.6	28.7	28.7	35.0	87.6	34.9	25.0
2-turn(1-4)	30.6	57.8	25.6	95.8	34.9	31.6	56.3	88.9	31.5	33.3
3-turn	35.3	36.0	64.6	88.7	37.0	33.8	44.9	57.6	93.5	36.1
4-turn	64.5	66.6	64.7	31.9	29.4	34.9	56.5	105.9	56.3	37.6
τ [O2-C1-C4'-O3']										
X-ray	-38.1	-39.1	-12.9	-75.2	143.4	-38.1	-39.1	-12.9	-75.2	143.4
1-turn	-61.8	-64.4	1.3	-89.8	101.3	-56.9	-60.2	-46.8	14.0	75.0
2-turn(1-5)	-78.0	-51.5	113.4	-64.4	-20.5	-53.0	-64.4	131.0	-49.3	-31.3
2-turn(1-4)	-40.1	-87.7	-31.7	134.3	-73.8	-69.4	-125.9	145.4	-13.4	-41.9
3-turn	-81.5	-4.4	-101.4	122.2	-58.8	-73.9	16.4	-101.5	131.2	-57.0
4-turn	-94.5	-105.7	-116.5	-68.9	-37.8	-59.8	-86.1	151.3	-88.1	-9.4

In the Table 4.2 the various conformations of CD10 are classified. For reason of comparison, the X-ray data are given as well. During the REMD simulation conformations with different numbers of glucose unit flips (turns) can be observed. As

mentioned above, two turns could be observed in the crystal structure, whereas the simulations show that there are more possibilities for the appearance of turns. The model 2-turn(1-5) represents a conformation similar to the crystal structure, whereas the 2-turn(1-4) conformation shows a larger and a shorter helical band of glucose units which are located in the macrocyclic ring. Conformations with higher numbers of turns are also found during the simulation, the smaller probabilities. In Figure 4.11, the probabilities of conformations with different numbers of turns are given for both, for the lowest simulation temperature (300K) as well as for some higher temperatures. At 300K conformations with 2 glucose flips are dominating to a high extent followed by 3-turn conformations. Only a very small number of conformations without a turn as well as conformations with more than 4 turns can be observed. Thus, obviously, it can be assumed that these conformations exist in a rapid dynamical equilibrium.

The temperature dependence of the distance probabilities (Figure 4.10) is in accordance with the distribution scattering increase due to temperature changes. In Figure 4.11, the distributions of various numbers of turns are given along the simulation times for four temperatures. The population of the number of turns is temperature dependent. The highest probability of the number of turns has the 2-turn system. These findings are correlating with the population of 0- and 1-turn conformations as well as conformations with higher number of turns. This means that conformations with other turn numbers than 2 are energetically less favored, and moreover, higher temperatures lead to higher populations of these energetically less favored conformations. In Figure 4.12 some examples of snapshot geometries are given for various types of turn-conformations. It can be seen that the conformation of a saddle-point structure, as

observed for the crystal structure, is existing for 1-turn, 2-turn and to some extent for 3-turn geometries, whereas higher numbers of turns lead to more flat conformations of the large ring system.

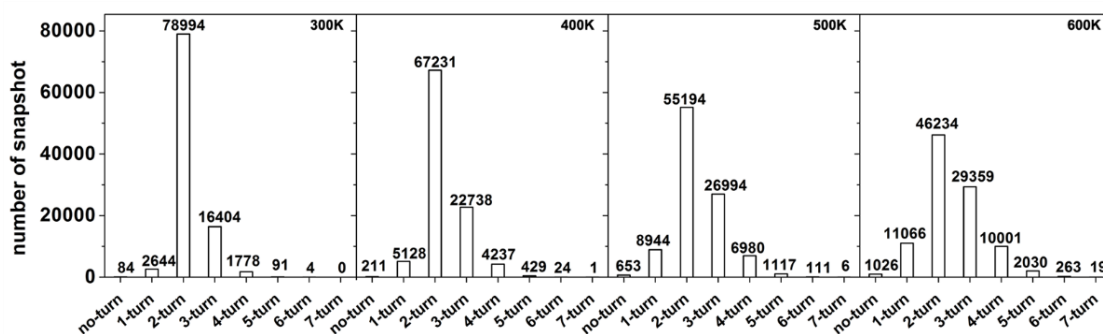


Figure 4.11 Probability of turn rotation of glucose units in CD10 ring at various temperatures

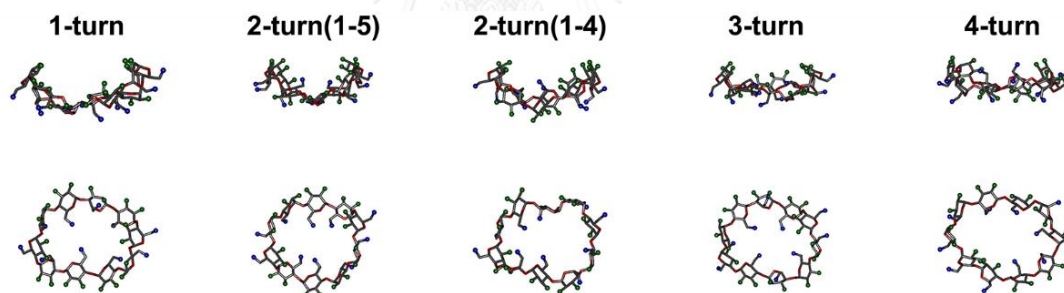


Figure 4.12 Examples for CD10 conformations with different numbers of turns, extracted from REMD simulation at 300 K

In Table 4.3 the probabilities of the different conformations obtained from the snapshots of the LR-system classified by the various turns are given. In REMD simulations, we could calculate differences in free energy and other thermodynamic properties among these conformations from these probabilities [108, 109]. Because the

2-turn model is the most dominant conformation, the free-energy difference ΔF of other $n - turn$ models from this model is given by

$$\Delta F = F_{n-turn} - F_{2-turn} = -RT \ln \frac{f_{n-turn}}{f_{2-turn}}, \quad (4.1)$$

where f_{n-turn} is the probability of n -turn conformation and R is the gas constant: $R=8.31$ J/(mol K). The energy difference results from the temperature dependence by

$$\Delta E = E_{n-turn} - E_{2-turn} = \frac{d(\frac{\Delta F}{T})}{d(\frac{1}{T})} = -R \frac{d(\ln(\frac{f_{n-turn}}{f_{2-turn}}))}{d(\frac{1}{T})} \quad (4.2).$$

Energy differences were calculated from a linear fitting of the data. The entropy term $T\Delta S$ can be calculated by

$$T\Delta S = \Delta E - \Delta F \quad (4.3).$$

These thermodynamic quantities are also listed in Table 4.3. It should be mentioned, that the 7- and 8-turn conformations are only observed at high temperatures with a very small probability. The corresponding thermodynamic properties were not calculated. Referring to the 2-turn conformations several arrangements are possible. The preferred conformation are given by 2-turn(1-5) and 2-turn(1-4) models showing also comparable probabilities.

Table 4.3 The probability distribution of CD10 conformation with different number of turns and the thermodynamics quantities ΔF , ΔE , and $T\Delta S$ at 300K

	Probability				ΔF at 300K (kJ/mol)	ΔE at 300K (kJ/mol)	$T\Delta S$ at 300K (kJ/mol)
	300K	400K	500K	600K			
no-turn	0.001	0.002	0.007	0.010	17.1	15.4	-1.7
1-turn	0.026	0.051	0.089	0.111	8.5	9.9	1.5
2-turn	0.790	0.672	0.552	0.462	0.0	0.0	0.0
3-turn	0.164	0.227	0.270	0.294	3.9	5.5	1.6
4-turn	0.018	0.042	0.070	0.100	9.5	11.2	1.7
5-turn	0.001	0.004	0.011	0.020	16.9	18.1	1.3
6-turn	0.000	0.000	0.001	0.003	24.7	23.6	-1.0
7-turn	–	0.000	0.000	0.000	–	–	–
8-ture	–	–	–	0.000	–	–	–

4.1.3) The conformation change of CD14

REMD simulations were performed on the larger ring size of CD14. To investigate the conformational changes of CD14, a new structure analysis using the degree of bending and its circularity are introduced. In addition, the thermodynamic quantities were also calculated. All REMD simulations of CD14 were performed by the same setups as the REMD of CD10. These REMD simulation conditions have been tested in the previous study on CD10, section 4.1.2 and ref. [110]. The 16 replicas under temperature exchanging within the range 300-600 K with 20 K interval of CD14 were simulated for 100 ns based on glycam06 and Igb5 of solvent GB model. By this REMD condition, the acceptance ratio is more than 40%. It can be seen that these REMD setups are suitable for CD14 conformation study as well.

Generally, CD14 conformations are bent along its diameter, resulting in a biplanar configuration. The X-ray structure of CD14 is depicted in Figure 4.13. In this type of structure, the degree of bending between the two planes significantly affects the inclusion ability of drug molecules. To systematically analyze the biplanar angle (θ_p) of large amount of CD14 conformations from REMD simulations, we have developed an algorithm and implemented it into a program that automatically measures biplanar angles of all CD14 conformations. This algorithm can be summarized in three steps as follows:

Step 1: Atoms within each CD14 molecule are clustered into two groups based on their spatial coordinates using k -mean clustering algorithm. In general, k -mean clustering is an optimization algorithm to cluster a set X of examples $x \in \mathcal{R}^m$ to k groups by minimizing the sum of distances between each example and its corresponding cluster centroid:

$$\min \sum_{x \in X} \text{dist}(f(C, x), x), \quad (4.4)$$

where C contains centroid of each cluster, $f(C, x)$ returns the nearest centroid in C to x based on Euclidian distance, and $\text{dist}(x, y)$ is the Euclidian distance.

Step 2: Each atom cluster is mapped onto a representative plane P_i for i -th cluster, such that it minimizes the sum of orthogonal distances of each atom in cluster i to P_i . To implement this concept, we performed a principle-component analysis (PCA) for each atom cluster. The two most dominant principle component axes represent orthonormal vectors spanning P_i and the third principle axis is the normal vector $\hat{\mathbf{n}}_i$ of P_i .

Step 3: Angle between plane P_1 and P_2 are calculated from cosine of their normal vectors. Noted that normal vector of each plane could be aligned in either positive or negative direction toward another plane. This makes the resulting cosine undistinguishable among the true biplanar angle θ_p and its supplementary angle $\pi - \theta_p$. In this study, we assume that the true angle of P_1 and P_2 is wider than its supplementary due to the stiffness of oligosaccharide chain. Thus, biplanar angle was calculated from $\max(\theta_p, \pi - \theta_p)$.

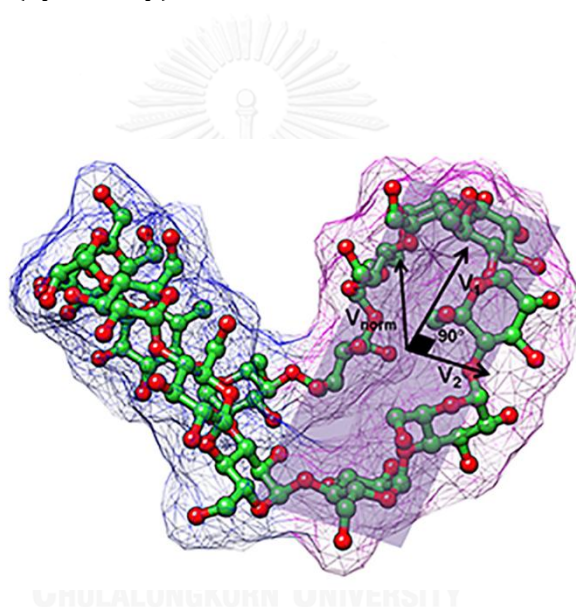


Figure 4.13 schematic diagram depicting the representative plane P_i (showed in purple color) of one atom cluster (purple cloud on the right), two-most dominant principle axes (v_1 and v_2), and v_{norm} as a normal vector to plane P_i .

As for circularity calculation, all diameters of CD14 are calculated from distance between each two O4 oxygen atoms on the opposite site of the CD14 ring (*i.e.* O4 atom of i -th glucose subunit and the O4 atom of $(i+7)$ -th glucose subunit). Circularity (γ_c) of CD14 is defined as a ratio between the minimum and maximum diameter of CD14 molecule (Figure 4.14).

$$\gamma_c = \left\{ \frac{\min_{i=\{\dots\frac{N}{2}\}} (r_{O_4}(i), r_{O_4}(i+\frac{N}{2}))}{\max_{i=\{\dots\frac{N}{2}\}} (r_{O_4}(i), r_{O_4}(i+\frac{N}{2}))} \right\}, \quad (4.5)$$

N denotes the number of glucose subunits in the cyclodextrin ring, $r_{O_4}(i)$ is the O_4 atom coordinate of the i -th glucose subunit. Based on this definition, circularity of CD14 is 1 when all diameters are exactly the same (perfect circular shape). Circularity is decreasing as the structure tends to be more elliptical shape.

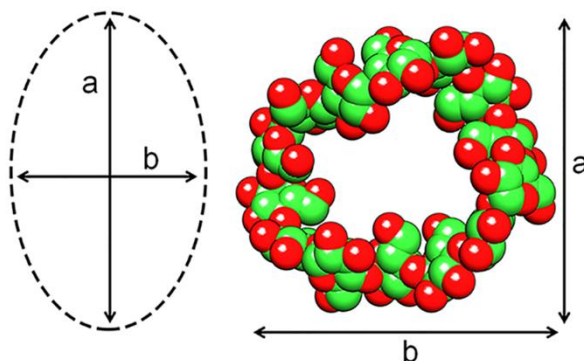


Figure 4.14 Schematic diagram depicting the ratio between the major and minor diameters of the ellipse on a 2D plane.

These two structural properties were analyzed based on 100000 REMD snapshots. The temperature dependence of CD14 structure is also considered. Based on Maxwell–Boltzmann statistics, the relative energy of CD14 was computed in comparison between each CD14 conformation according to their biplanar angle (θ_p) or circularity (γ_c^2).

The bending of CD14 structure can be defined by the biplanar angle θ_p . The MD snapshots were extracted from each θ_p range, CD14 which has $90 \leq \theta_p \leq 180$ are divided into 9 ranges according to their biplanar angle with 10 degree interval, defined

by $\theta_P(1)$ - $\theta_P(9)$. Ten representative structures of CD14 in $\theta_P(1)$ - $\theta_P(9)$ were superimposed as displayed in Figure 4.15. The CD14 structures preferred to have the θ_P in range of 140-150 degrees, $\theta_P(6)$ in all designed temperatures (the details of temperature dependence of CD14 conformations will be mentioned later). From Figure 4.15, the difference of CD14 bending in each range can be clearly seen. However, their structures in the same range, for example $\theta_P(8)$ are not comparable, as one can see from the ring shape given in Figure 4.15. Therefore, the ring roundness as CD14 circularity (γ_c^2) is additionally calculated.

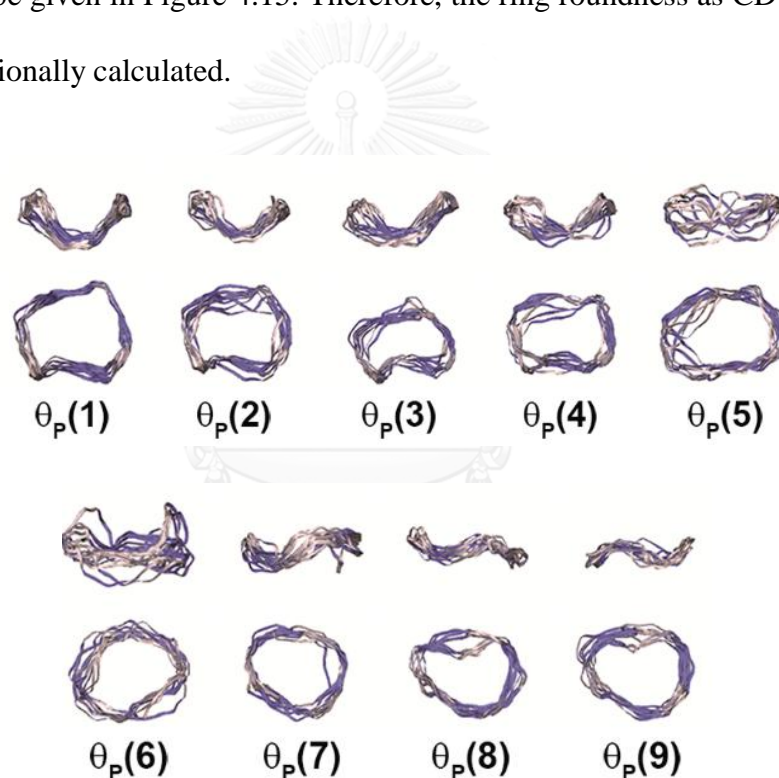


Figure 4.15 Examples for CD14 structures with various biplanar angle; $\theta_P(1)$ - $\theta_P(9)$, extracted from REMD simulation at 300 K

The CD14's cavity shape can be described by the γ_c^2 . Both cyclic and elliptic ring conformations could be possibly formed due to the higher flexibility of CD14 compared to SR-CDs as well as CD10 (Figure 4.16). The CD14 structures were

considered according to their circularity changes. CD14 behaves like a cyclic when γ_c^2 approach to one. The CD14 structures were classified by γ_c^2 into 10 groups where $0 \leq \gamma_c^2 \leq 1$ with 0.1 interval *i.e.* $\gamma_c^2(1)$ - $\gamma_c^2(10)$. At low γ_c^2 , CD14 exists in an elliptic shape and induces a 2-loop-like conformations as seen by snapshots of $\gamma_c^2(1)$ and $\gamma_c^2(2)$ range. The perpendicularity between these two loops could be observed for $\gamma_c^2(2)$. Apparently, the almost perfect cyclic CD14 with single cavity was shown when the γ_c^2 is closed to 1 as CD14 in $\gamma_c^2(8)$ - $\gamma_c^2(10)$ range.

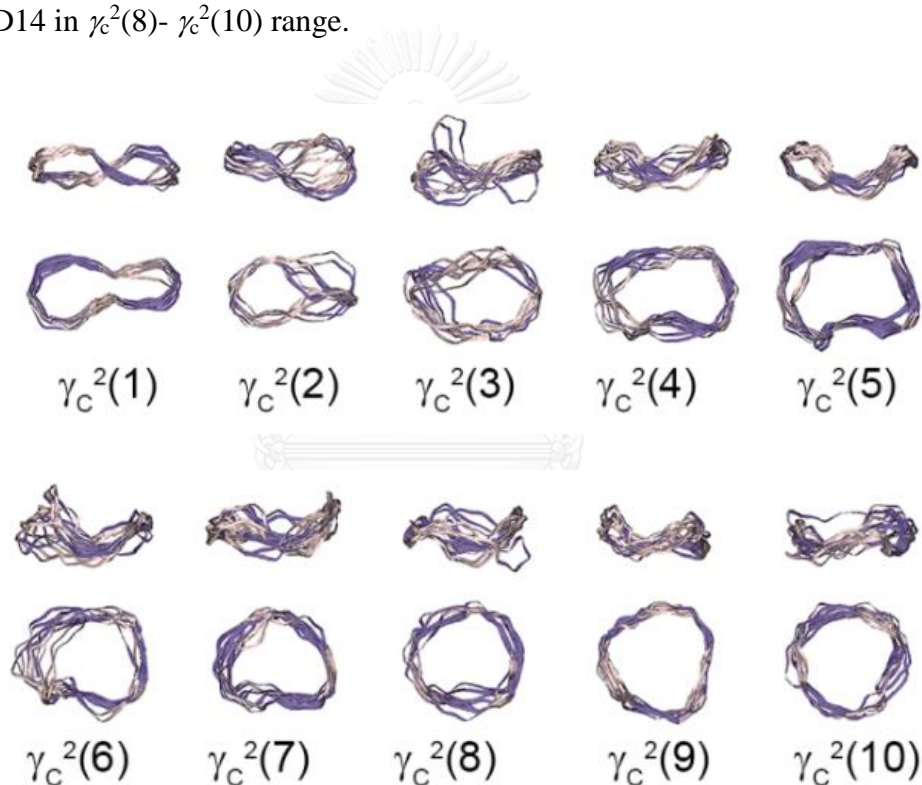


Figure 4.16 Superimposition of 10 MD snapshots of CD14 at 300 K according their circularity change; $\gamma_c^2(1)$ - $\gamma_c^2(10)$

The relative free energy of CD14 deformations at 300 K were independently estimated for θ_P and γ_c^2 changes. In Figure 4.17, the free energy of CD14 of each range $\theta_P(1)$ - $\theta_P(9)$ and $\gamma_c^2(1)$ - $\gamma_c^2(10)$ was compared to the free energy of the most possible

range *i.e.* $\theta_P(6)$ and $\gamma_c^2(4)$, respectively. The results showed that the free energy changes of CD14 of each θ_P and γ_c^2 range were lower than 8 kJ/mol and 18 kJ/mol, respectively. It can be suggested that it is easy to transform their bending both for tight bent-form and opened-form switching. The change of the most stable $\theta_P(6)$ to the flat CD14 of $\theta_P(9)$ is more favorable than to the tight bend of $\theta_P(1)$. While the double free energy is required for transformation of the most stable $\gamma_c^2(4)$ to cyclic CD14 with respected to the elliptic ring deformation.

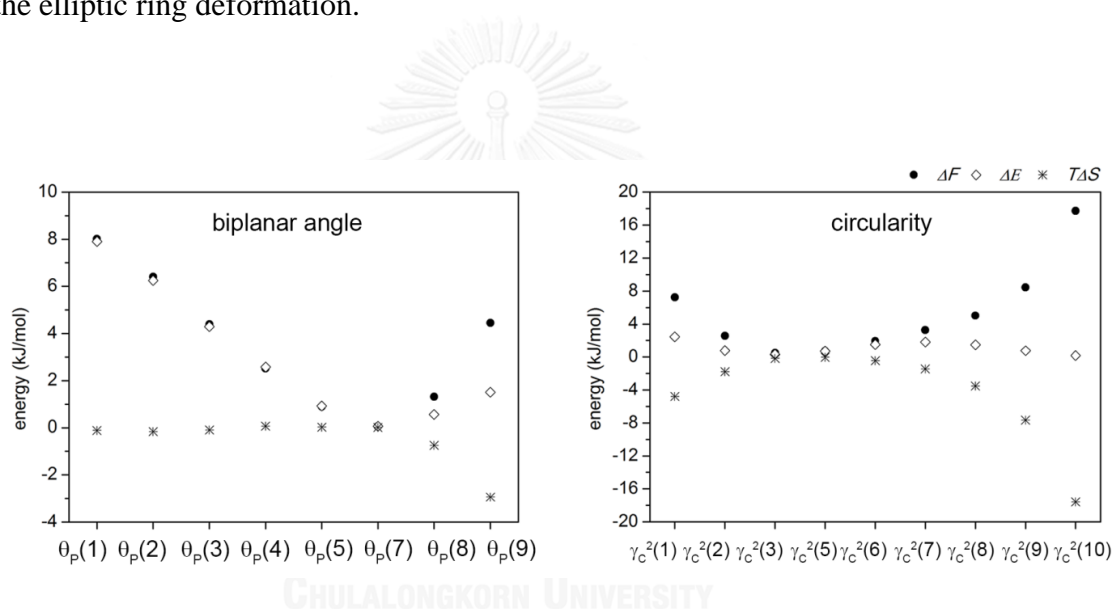


Figure 4.17 The thermodynamics quantities ΔF , ΔE , and $T\Delta S$ at 300K of CD14 conformations

The temperature dependence of CD14 conformations was investigated. The distribution of biplanar angle (θ_P) and circularity (γ_c^2) for all designed temperatures are shown in Figure 4.18(a) and 4.18(b), respectively. With the analytical result of 100,000 CD14 structures, the biplanar angles around 140-160 degrees are favored by 54-67% of all CD14 structures. The temperature dependence was shown as the decreases of biplanar angles at high temperature. When the temperatures are higher than 320K, the

peaks slightly shifted to have lower biplanar angle with 4-23% decreasing of the number of the CD14 structures in the most probable range compared to the simulation of 300K. Consequently, the probabilities of 90 and 180 degree plane angle at high temperature were significantly increased, especially the 90 degree bent form which is 252% increased at 600K, for instance. The findings suggested that the CD14 prefer being in the bent form, however, the conformation changes to tight bent shape or flat shape could be enhanced by temperature increase. Similarly, the CD14 was mostly distributed by 43-49% in range of $0.275 < \gamma_c^2 < 0.425$ of γ_c^2 referring the non-cyclic shape of CD14. These most probable structures were slightly decreased at higher temperatures. Almost temperatures at higher than 300K, except for 320K and 460K increased the CD14 elliptical ring favor where $0.025 < \gamma_c^2 < 0.175$, conversely the temperature effect on cyclical-liked ($0.825 < \gamma_c^2 < 0.975$) is insignificant.

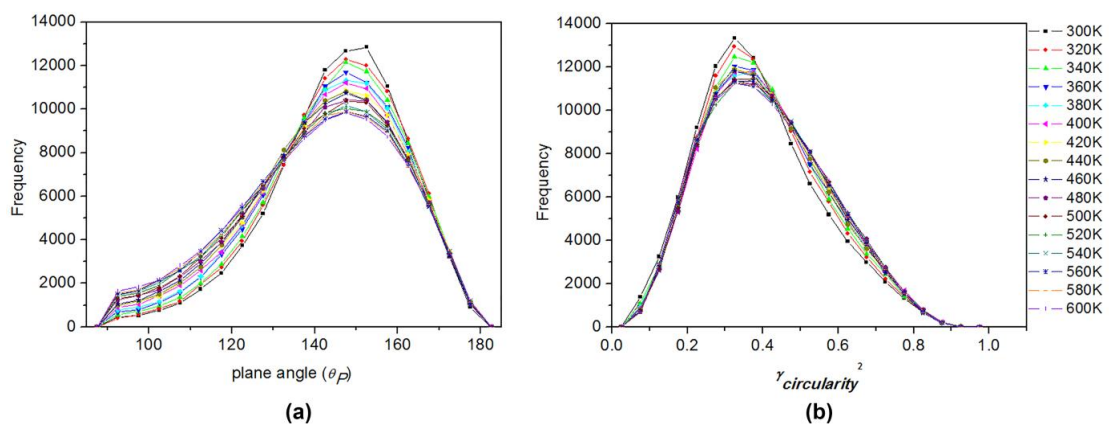


Figure 4.18 Distribution plots of (a) biplanar angle (θ_p) and (b) circularity (γ_c^2) for all designed temperatures

Based on 2D distribution plots of these two parameters (Figure 4.19), the MD snapshots of CD14 simulation at 300K were extracted from different locations (S1-S16,

defined in Figure 4.19 at 300 K). Also the 2D contours of other temperatures are compared. The same size of sampling area, which is ± 10 and ± 0.01 for θ_P and γ_C^2 , respectively were used. The 10 representative snapshots of each sampled locations are superimposed as illustrated in Figure 4.20.

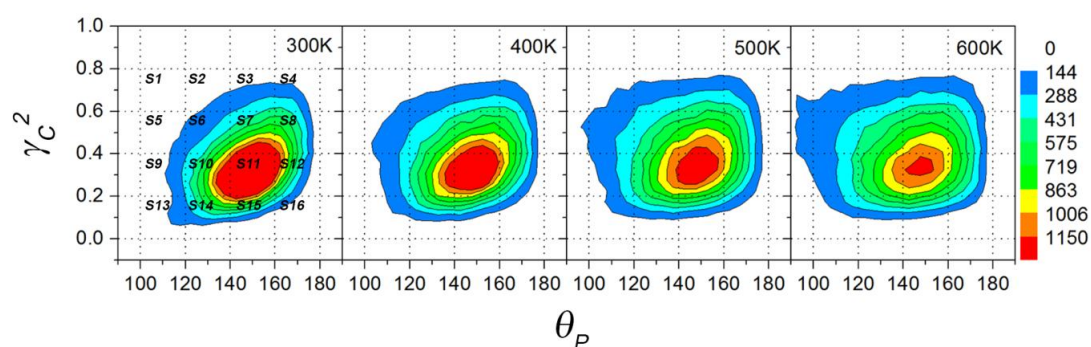


Figure 4.19 2D contours between the θ_P and γ_C^2 where the probabilities of CD14 in each region are labeled with blue to red color for low to high value, the 16 sampling area is remarked in 2D plot of 300K, defined by S1-S16.

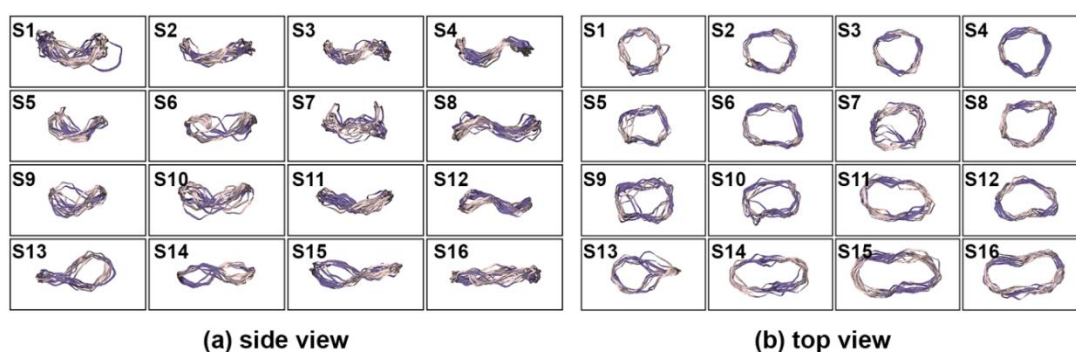


Figure 4.20 Superimposition of the 10 representative MD snapshots in each possible CD14 conformation (S1-S16) i.e. S11 is the most probable CD14 conformations (opened-form), S1 and S5 are closed-form, S3, S4, S8 and S12 are asymmetric bent form, and S13-S14 are 2-loops-like form

The contour plots show that the CD14 mostly located at $(\theta_p, \gamma_c^2) \sim (150, 0.3)$ for all temperatures. The ring-opening was investigated according to their biplanar angle enlargement compared with X-ray structure which have $(\theta_p, \gamma_c^2) \sim (105, 0.4)$ as shown in Figure 4.20, S11 is defined as opened-form. The temperature increase changed somewhat the expanded distribution at S1, S2 and S5 area in Figure 4.20, as clearly seen by the 2D-plot of the simulation at 600K. As expected, CD14 could generate more various structures not only of symmetric bent form with one cavity, but also we observed other conformations with one cavity with asymmetric bent shape (Figure 4.20, S3, S4, S8 and S12) as well as CD14 with more than one cavity as 2-loops shape (Figure 4.20, S13-S14). Interestingly, the perfect helix CD14 like double-stranded DNA could be observed in the S14 sample range, which has $(\theta_p, \gamma_c^2) = (124.051, 0.072)$. These opened-form and 2-loops conformation was also found by classical MD simulation [34]. Moreover, the temperature effect on each CD14 conformation was newly analyzed in Figure 4.21. The plots show that the probability of opened-form (S11) is decreased and subsequently the closed-forms (S1 and S5) are increased at the high temperature. However, there is no significant effect to other conformations of asymmetric bent and 2-loops shape.

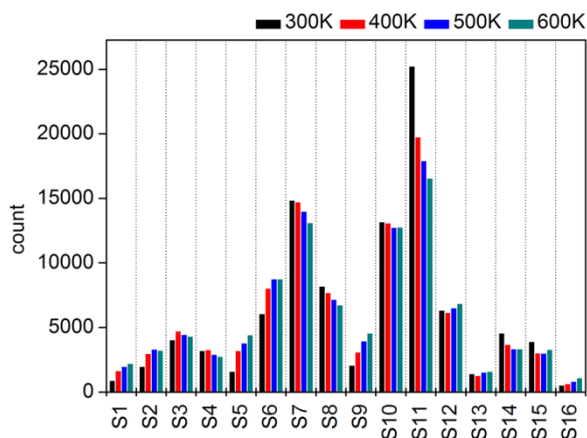


Figure 4.21 Temperature dependence of CD14 in each conformation S1-S16

4.2) Part II: Study of permeation mechanism of beta cyclodextrin and its derivatives to the biological membrane

Here, we aim to visualize the permeation behavior of β CD on POPC lipid bilayer. The influence of chemical structures of β CD and some substituted derivatives on the interaction with the cellular membrane was investigated by MD simulations. The understanding of the β CD-lipid interaction correlating to drug releasing behavior is expectation. The results of this study have been divided into four sections as follows:

4.2.1) *The permeation and insertion of β CD into the lipid bilayer*; the permeation of β CD into the POPC lipid bilayer and the effect of β CD molecule insertion on the bilayer were shown. 4.2.2) *The interaction of β CD with the lipid bilayer*; the hydrogen bond formations was investigated to determine the binding affinity between β CD and lipids. In addition, the influence of β CD on lipid bilayer properties were analyzed in terms of 2D-density map of POPC phosphorous atoms and lipid thickness. 4.2.3) *The conformational change of β CD in lipid bilayer*; the conformation and structural

stability of the β CD at water, water-lipid interface and lipid bilayer were considered. And the last section, 4.2.4) *The influence of chemical modification of β CD on membrane permeability*; the interaction of β CD derivatives (ME β CD and HP β CD) with the lipid bilayer were studied. The permeation depth was considered according to the substitution type and position.

4.2.1) *The permeation and insertion of β CD into the lipid bilayer*

Multiple MD simulations taking into account various configurations of β CD with POPC lipid bilayer were performed starting from various positions, assigned by BCD1-BCD5 system. The orientation and position at lipid bilayer of β CD molecule was varied as shown in Figure 3.2. For systems BCD1-BCD3, β CD was initially set far away from the bilayer center (around 3.5 nm) (as seen in Figure 4.22(a)) to avoid the bias of the interactions between the β CD and the lipid bilayer. This allowed the β CD molecule to move and to rotate freely in aqueous solution before approaching the bilayer surface. To study the permeation of β CD into the lipid bilayer, the distances at the z-axis between β CD ($r_{\beta CD}$) and its rims ($r_{P\beta CD}$ and $r_{S\beta CD}$ for primary and secondary hydroxyl sides, respectively) away from the lipid bilayer's center were determined. The center of mass (COM) of all lipid molecules, the COM of all atoms in the β CD molecule, the COM of C5 and O5 atoms, and the COM of C2 and C3 atoms were defined as the bilayer center, the β CD center, the primary rim center and the secondary rim center, respectively. The tilt angle of the β CD molecule is characterized by the angle between vector \vec{r} (the vector pointing from the COMs of the primary to the secondary rims and the bilayer normal). The definitions of all mentioned parameters are

illustrated in Figure 4.22(a) and Figure 4.22(b). The permeation behavior of β CD was described by the time dependence of those distances and its tilt angle for the first 350 ns (Figure 4.23). The complete analysis of the micro-scale simulations are collected in Figure 4.24.

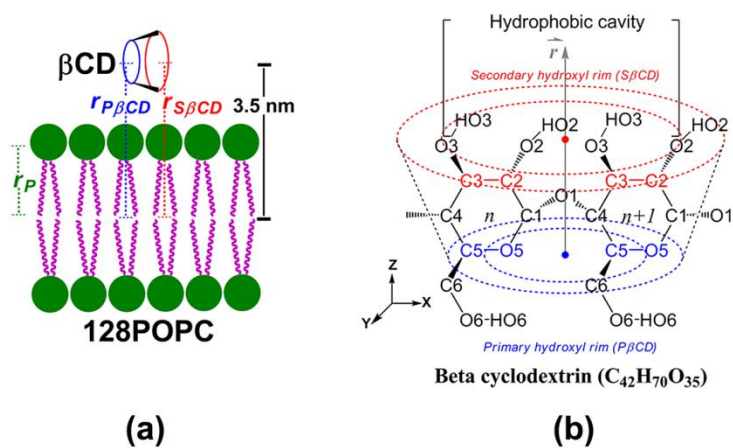


Figure 4.22 (a) Definition of analysis parameters; $r_{\beta CD}$, $r_{P\beta CD}$, $r_{S\beta CD}$ and (b) vector \vec{r} for tilt angle calculation

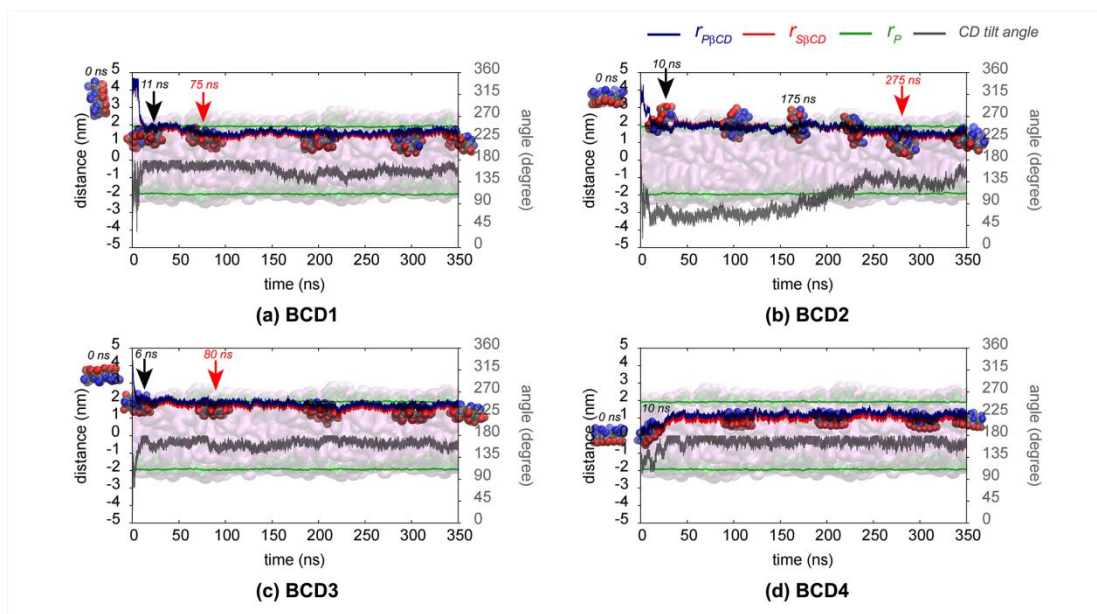


Figure 4.23 Closed-up for the first 350 ns of the permeation of β CD into the lipid bilayer for four simulations (BCD1-BCD4) using different initial structures. The distances as a function of time between the centers of bilayer and both rims of β CD molecule *i.e.* primary rim; $r_{P\beta CD}$ (blue) and secondary rim; $r_{S\beta CD}$ (red) are depicted. The β CD tilt angle and the distances of phosphate groups from the center of bilayer for both leaflets (r_P) are plotted in gray and green, respectively. The snapshots of β CD at different simulation time are enclosed in the plots where the blue and red balls represent the atoms of the primary and secondary rims, respectively. The lipids of the bilayer are shown by purple rods while their phosphorus atoms are depicted in green balls. The black and red arrows indicate the approaching and permeating time of β CD to the bilayer, respectively.

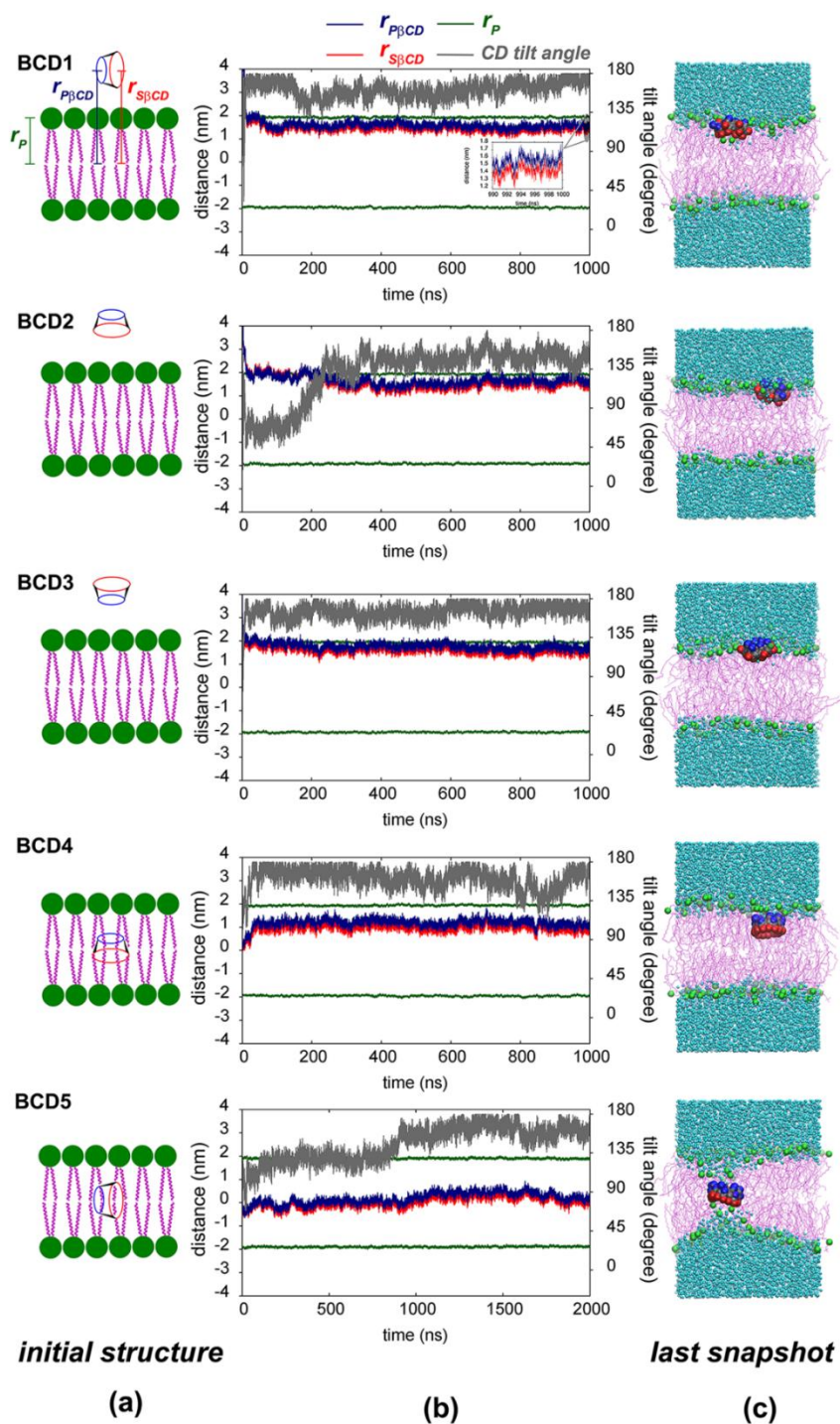


Figure 4.24 The association behavior of β CD on POPC bilayer of BCD1-BCD5 system for the whole simulation

Figure 4.23 shows that the β CD molecule in aqueous phase spontaneously moved toward the POPC bilayer and approached to the bilayer surface within the first 15 ns. For BCD1 and BCD3 systems, the β CD molecule attached to the bilayer with the secondary rim and readily permeated into the lipid bilayer within approximately 100 ns. The β CD remained underneath the phosphate group for the rest of the simulation time (Figure 4.24). For the BCD2 system, the β CD molecule firstly approached to the bilayer surface with the primary rim but it did not permeate into the bilayer over a hundred nanoseconds. After 175 ns simulation time, the β CD molecule rotated to have the secondary rim associated with the bilayer surface with the consequence of the β CD permeation within a few tens of nanoseconds as illustrated in Figure 4.23(b). After 500 ns, all β CD molecules are located in the region between phosphate and glycerol-ester groups with the orientation of the secondary rim pointing toward the bilayer center, although starting from the various geometries (Figure 4.24 and 4.25). The averaged distances between COMs of the β CD molecule and the bilayer as well as the tilt angle of β CD molecule with respect to the bilayer are presented in Table 4.4. In agreement with our results, the adsorption of β CD molecule at the monolayer/water interface with high affinity was observed by López et al. and it was related to the efficiency of cholesterol extraction from the monolayer by β CD [25]. Based on spectroscopic study and *ab initio* calculations, Mascetti et al. suggested that the β CD molecules preferred to stack in parallel to the pure cholesterol, mixed DMPG/cholesterol, and mixed DMPC/cholesterol lipid monolayers [111].

Next, the behavior of the β CD molecule and the effect of β CD insertion inside the bilayer were studied. Therefore, β CD was placed at the bilayer's center with the \vec{r} vector alignments in parallel (BCD4) and perpendicular (BCD5) to the bilayer normal. For BCD4 system, the β CD molecule is able to form hydrogen bonds with the glycerol-ester groups of lipid bilayer and moved toward the water-lipid interface within 10 ns (in Figure 4.23(d)). The equilibrium location of β CD was 1.0 nm from the bilayer center corresponding to the position of the glycerol-ester group. No bilayer deformation has been observed within a simulation time of one microsecond. Unlike the BCD5 system (Figure 4.26), the β CD molecule was initially oriented in perpendicular to the bilayer normal, therefore, hydroxyl groups of the β CD formed hydrogen bonds with the lipid heads of both bilayer leaflets. At longer simulation time, the β CD molecule rotated to be in parallel to the bilayer normal and a water pore formation across lipid bilayer could be observed (Figure 4.26(b)).

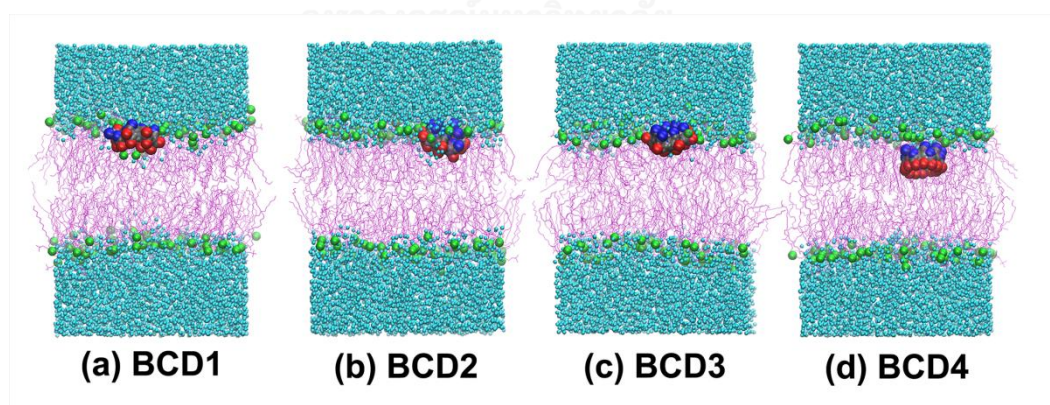


Figure 4.25 The last snapshots of BCD1-BCD4 simulations were extracted at 1 μ s. The primary rim of β CD, secondary rim of β CD, phosphorus atoms of lipid and water

molecules are presented by blue, red, green and cyan spheres, respectively. The purple lines represent the POPC lipid molecules.

Table 4.4 Average values of the focused parameters on β CD-lipid interactions for all simulations (BCD1-BCD5) over the MD production period

systems/properties	$r_{\beta CD}$ (nm)	$r_{P\beta CD}$ (nm)	$r_{S\beta CD}$ (nm)	tilt angle (degree)
BCD1 (500-1000 ns)	1.50±0.10	1.54±0.10	1.40±0.10	163.6±8.0
BCD2 (500-1000 ns)	1.55±0.13	1.61±0.13	1.49±0.13	148.8±7.6
BCD3 (500-1000 ns)	1.65±0.12	1.72±0.12	1.54±0.12	167.4±5.9
BCD4 (500-1000 ns)	1.08±0.13	1.17±0.13	0.96±0.13	157.0±11.1
BCD5 (1000-2000 ns)	0.30±0.14	0.37±0.15	0.20±0.12	161.4±7.4

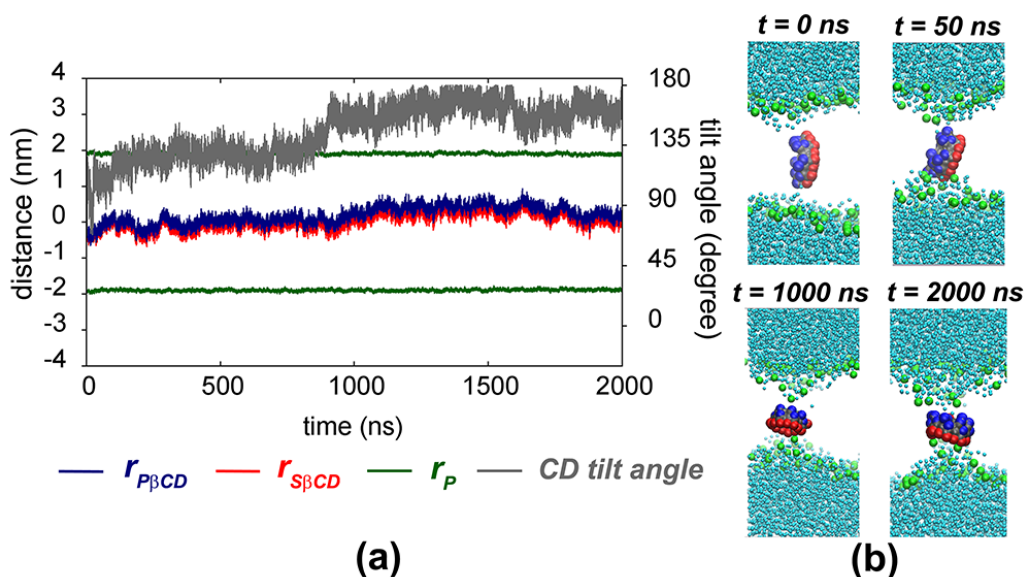


Figure 4.26 (a) Dynamics behavior of β CD starting from the perpendicular orientation in the lipid bilayer (BCD5). (b) Water pore formation induced by β CD at longer simulation time, where the cyan sphere represents the water molecules, while the blue, red and green spheres are symbolized as the atoms on primary and secondary rims of β CD and phosphorus of lipid head groups, respectively.

4.2.2) The interaction of β CD with the lipid bilayer

To determine the binding mode and the binding affinity of associated β CD on lipid bilayer surface, the number of hydrogen bonds (H-bonds) between β CD, its rims and the components of lipid head groups (phosphate and glycerol-ester moieties) were calculated using the usual geometric restrictions for hydrogen bonding. A hydrogen bond is defined by the distance between the donor and the acceptor (r_{HB}) < 0.35 nm and the deviation from the linearity $< 30^\circ$. The distance value of 0.35 nm corresponds to the first minimum of the radial distribution function (RDF) of water. Figure 4.27 shows the

average number of hydrogen bonds at the last 500 ns and 1 μ s for the systems of BCD1-BCD4 and BCD5, respectively. The β CD molecules in the BCD1-BCD3 systems interacted to the lipid head group with the hydroxyl groups at the secondary rim and it was more preferred to form hydrogen bonds with phosphate groups than with glycerol-ester groups. In contrast to the BCD4 and BCD5 systems, the primary rim of β CD is associated with the glycerol-ester group of the lipid bilayer. This is in good agreement with the results of the simulation snapshots and the permeate depths of β CD molecule into the bilayer. Interestingly, the number of hydrogen bonds of β CD with water molecules significantly decreased from 16 to 5 when the β CD molecule translocated from water-lipid interface into the bilayer. In conclusion, the results of the hydrogen bonds suggest that a deeper translocation of β CD into the hydrophobic region of the lipid bilayer is unfavorable [112].

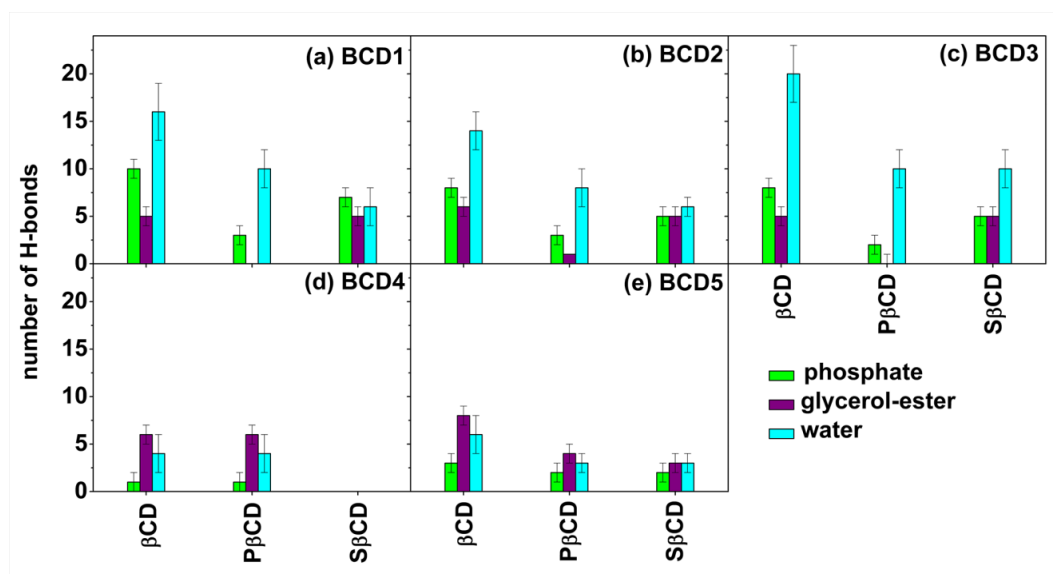


Figure 4.27 Hydrogen bond contribution of the interactions between the β CD molecule and phosphate (green) and glycerol-ester groups (purple) of the lipid and the solvating water molecules (cyan)

To search for the influence of β CD on lipid properties, the 2D-density map of the β CD molecule and the POPC phosphorus atoms, and the bilayer thickness based on Voronoi analysis [113] for the representative systems BCD3-BCD5 were plotted in Figures 4.28 and 4.29, respectively. As expected, the adsorption of only one β CD molecule on the lipid bilayer cannot deform the membrane structure as seen by insignificant changes of the 2D-density map and the lipid thickness of the BCD3 POPC membrane bilayer relative to POPC alone. The association of β CD on lipid surface slightly induced membrane pressing at the β CD located area. β CD positioned deeper in the BCD4 bilayer ($r_{\beta CD}$ of ~ 1.08 nm) even caused less interference on the structural properties of the lipids. In contradictory, the large distribution of phosphorus atoms

towards lipid interior and the dramatic change in lipid thickness were presented due to the transient water pore induced by β CD in the BCD5 system.

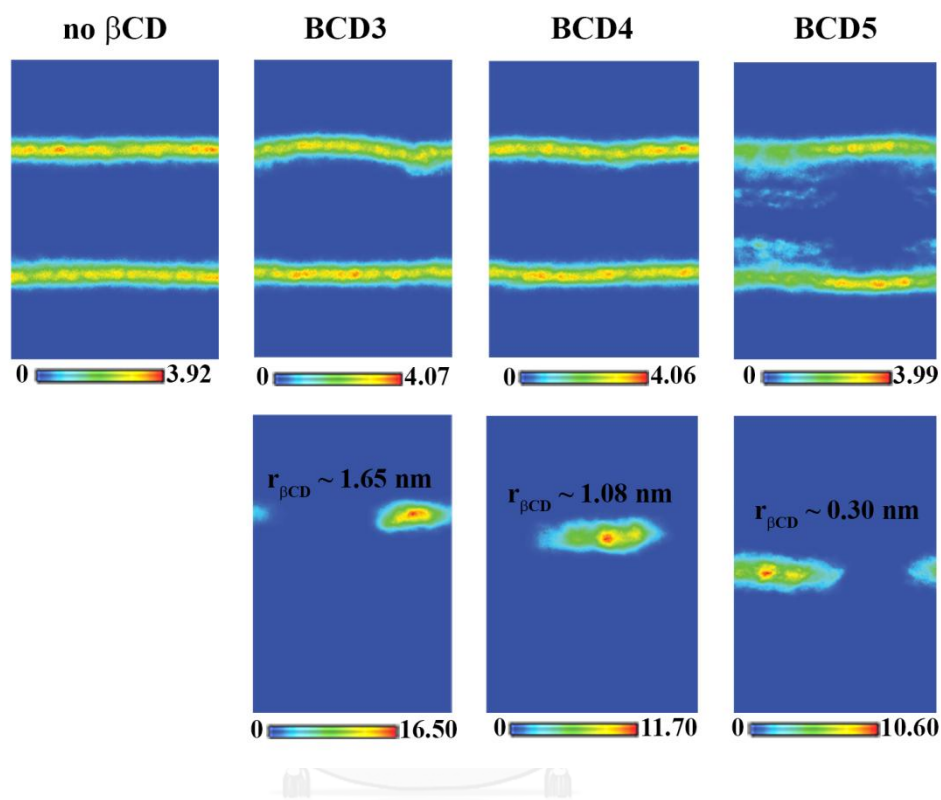


Figure 4.28 2D-density map on xz-plane of the POPC phosphorus atoms (top) and the β CD molecule (down) for representative BCD3-BCD5 systems, while that of the phosphorus atoms of POPC bilayer alone was given for comparison. The averaged distance between the centers of bilayer and β CD ($r_{\beta CD}$) is also shown

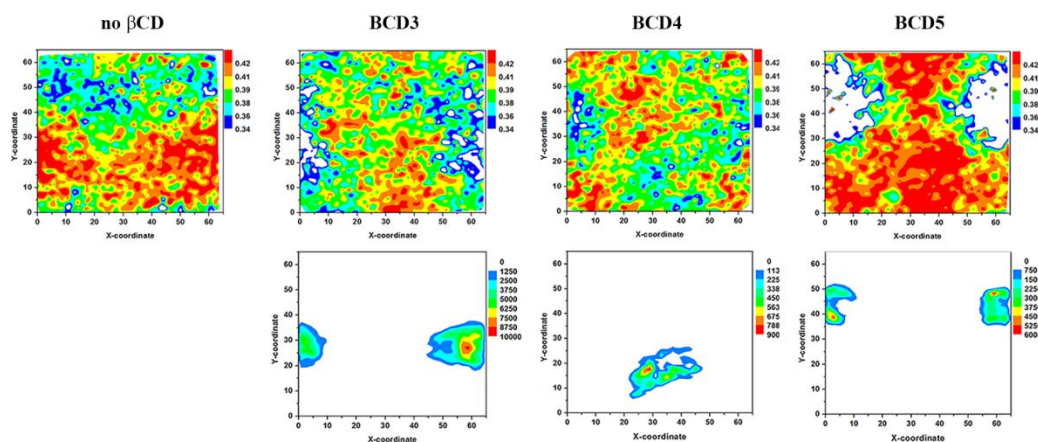


Figure 4.29 (Top) local lipid thickness of the POPC membrane bilayer in the systems without and with β CD (no β CD and BCD3-BCD5). (Bottom) 2D-frequency distribution of the β CD molecule in the BCD3-BCD5 systems

4.2.3) The conformation of the β CD change in lipid bilayer

To investigate the conformational change of the β CD molecule, we determined the intramolecular hydrogen bonds obtained by the number of hydrogen bonds of the secondary rim between the adjacent glucoses. The intramolecular hydrogen bonds are related to the stability of the CD molecule [32, 114]. The number of the intramolecular hydrogen bonds of BCD1-BCD3 systems was decreased continuously until there are no bonds left when the β CD molecule was attaching to the bilayer surface. The loss of this interaction was due to the preferable hydrogen bond formation between β CD and lipid head groups as well as water molecules [115-118] (Figure 4.27) and resulted in the structural deformation in Figure 4.30. The root mean square displacement (RMSD) of the hydroxyl side chains on each rim and glycosidic oxygens (O1) with respect to its anhydrous structure (in Table 4.5) showed that the primary rim of β CD was more flexible than the other one [118]. The solvating water molecules affected the flexibility

of the β CD structure for both side chain rims and the O1 core. In addition, the area of β CD cavity was calculated by the following equation:

$$A = \frac{\pi}{7} \sum_{i=1}^7 r_i^2, \quad (4.6)$$

where r_i is the distance between each hydroxyl group and the center of O1 atoms, and the hydroxyl groups at 6- and 3-positions are used for representing the cavity area of primary and secondary rims, respectively. The cavity areas of β CD molecule in water, water-lipid interface and lipid phase were summarized in Table 4.5. As expected from the truncated cone geometry of the β CD molecule, the cavity area of the secondary rim was larger than that of the primary rim about 1.5 fold in water and lipid phases, whereas the shape of the β CD molecule in the lipid tail resembled to a cylinder. The area cavities of the secondary rim in lipid phase were ~15 % and ~25% smaller than in water and water-lipid interface, respectively. These finding may be related to the mechanism of drug release in which the open and closed states of the secondary rim of the β CD molecule at different phases play an important role.

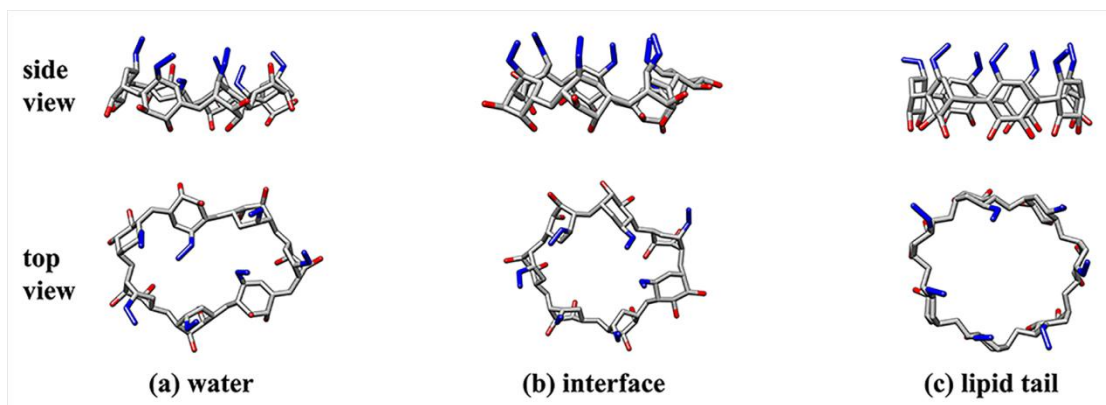


Figure 4.30 The β CD in water was independently simulated for 500 ns, and the last MD snapshot is shown in (a). The last snapshots of β CD molecules obtained from the simulations of BCD3 and BCD4 for representing the β CD structure in lipid-water interface and lipid tail region are depicted in (b) and (c), respectively. The primary and secondary rims of β CD molecule are labeled in blue and red, respectively. The backbone atoms of β CD molecules are represented in gray.

Table 4.5 The RMSD and cavity area of β CD molecule on each hydroxyl rim

Systems	$r_{\beta CD}$ (nm)	RMSD (nm)			Cavity Area (nm ²)		
		O1	1st	2nd	O1	1st	2nd
In water	-	0.12±0.02	0.33±0.04	0.25±0.02	0.93±0.04	1.19±0.12	1.56±0.11
At	1.59±0.10	0.10±0.01	0.29±0.01	0.23±0.01	0.86±0.03	1.36±0.06	1.69±0.03
In lipid tail	1.00±0.10	0.06±0.01	0.17±0.02	0.08±0.02	0.80±0.02	1.35±0.07	1.35±0.04

4.2.4) The influence of chemical modification of β CD on membrane permeability

The independent micro-scale MD simulations of β CD derivatives as ME β CD and HP β CD interacting with POPC lipid bilayer were performed to study the effect of

modified β CD on its membrane permeability. The substitution effect of modified β CD according to their chemical functions and substitution position were taken into account. The methoxy groups ($-\text{OCH}_3$) and 2-hydroxypropyl groups ($-\text{OCH}_2\text{CH}(\text{OH})\text{CH}_3$) were substituted at 2- or 6- or 2, 6-position of hydroxyl groups on all glucose subunits of regular β CD to form ME β CD and HP β CD derivatives, respectively. The initial setup details are described in Table 3.1. Multiple initial conformations with several orientations and positions of β CD derivatives at the lipid bilayer were conducted like the simulations of regular β CD (Figure 3.2), designed by BCD1-BCD5 systems.

The permeation behaviors of ME β CD and HP β CD on POPC lipid bilayer were described by the distances between the β CD derivatives and the lipid bilayer center. The averages of $r_{\beta\text{CD}}$, $r_{P\beta\text{CD}}$ and $r_{S\beta\text{CD}}$ of each β CD derivatives system for 500 ns at last are plotted, compared to those distances of the regular β CD simulations (Figure 4.31). All definitions of the distances correlated with the analysis of regular β CD simulations (Figure 4.22). The distances between the COM of POPC bilayer and *i*) the COM of all atoms of β CD derivatives, *ii*) the COM of C5 and O5 atoms of β CD derivatives and *iii*) the COM of C2 and O3 atoms of β CD derivatives were defined as $r_{\beta\text{CD}}$, $r_{P\beta\text{CD}}$ and $r_{S\beta\text{CD}}$, respectively. The results showed that these two substitutions as well as their substituted positions on β CD derivative molecule affected their permeation depth. As for the methoxy-group substitution, a deeper permeation of ME β CD was found when the association of the secondary rim of ME β CD on lipid surface is preferred. However, the interaction of methyl groups and lipid polar groups is less favorable compared to non-modified β CD, except for the secondary rim approaching of 2-ME β CD in system

BCD2 and BCD3. In case of HP β CD, the long chain of hydroxypropyl induced the deep permeation of HP β CD into lipid bilayer. The permeability of substituted β CD at the same positions of hydroxypropyl is higher than that methoxy replacement of ME β CD, except for the substitution at 2-position. The deepest permeation was found for 2,6-HP β CD, with a value around 1.13 nm. Due to steric effects of the substituted side chains of 2,6-HP β CD, the conservation of 2,6-HP β CD orientation of the initial structure was observed during simulation. Besides, the insertion of β CD derivatives into the lipid bilayer was investigated by simulations starting from BCD4 and BCD5 systems. The interaction of β CD derivatives and the non-polar region of lipid tails are unfavorable. ME β CD in any case moved up from the bilayer center to interact with the lipid head groups. This behavior was also found for 2-HP β CD and 6-HP β CD where the HP β CD was originally placed at the bilayer center with parallel orientation in the system BCD4. The last snapshots of simulations of ME β CD and HP β CD derivatives are illustrated in Figure 4.32 and Figure 4.33, respectively.

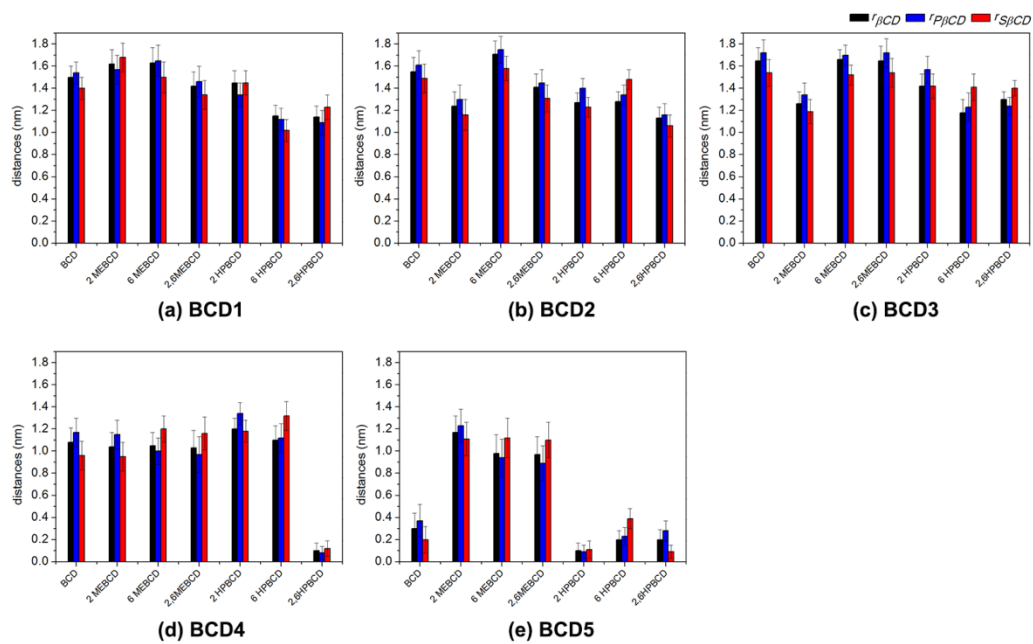


Figure 4.31 The average of $r_{\beta CD}$ (black), $r_{P\beta CD}$ (blue) and $r_{S\beta CD}$ (red) for all βCD derivatives in BCD1-BCD5 system

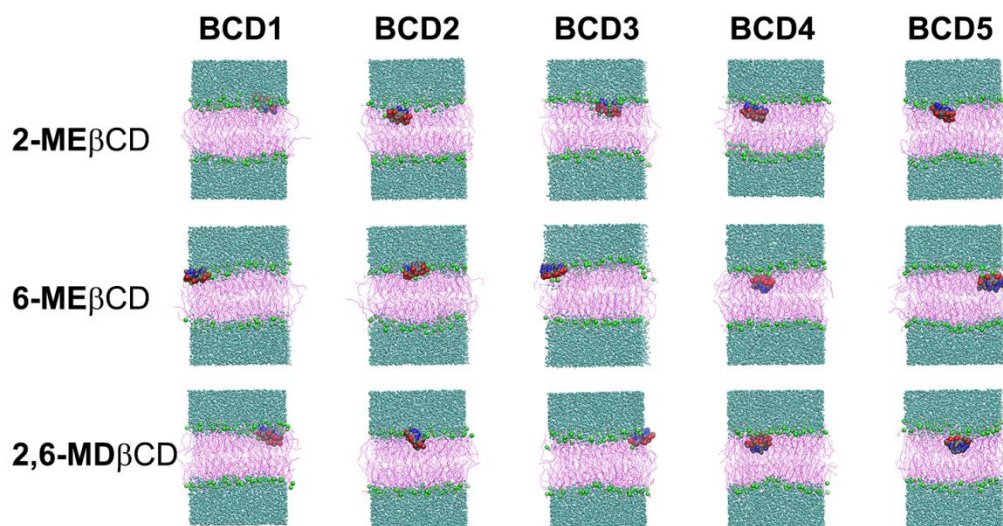


Figure 4.32 The last snapshots of ME β CD simulations

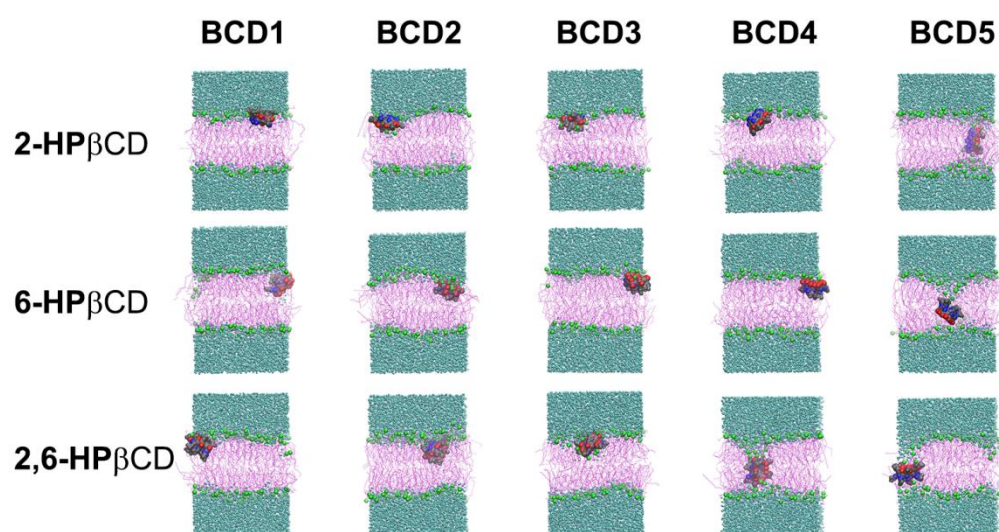


Figure 4.33 The last snapshots of HP β CD simulations



CHAPTER 5

CONCLUSIONS

The understanding of cyclodextrin conformation diversity and the membrane permeability could be provided by molecular dynamics simulations. Our research highlights are the force field validation for REMD simulation of CDs, the diversity of CD structures and the permeation behavior of CDs through lipid membrane. In the first part, the possible conformations of CDs were investigated by their structural analysis obtained from REMD simulations. And the second part, the micro-scale MD simulations were used to visualize how β CD permeates into lipid bilayer.

First, to study the conformation diversity of CDs, we performed the REMD simulations for 100 ns on various sizes of CDs: CD6, CD7, CD8, CD9, CD10 and CD14. To get the reasonable REMD results, some important simulation setups such as the force field, GB solvent model, the replica number and simulation temperature range were verified on the representative simulation of CD10. The overlapping of potential energies between each replica as well as the structural properties of the O2-O3 and O4-O4 distance referring the flip character and ring shape, respectively were taken into account. By doing so, the sixteen replicas in the temperature range of 300 K to 600 K could afford the reliable results for all CDs sizes when the glycam06 force field and Ibg5 implicit solvent model were used in the simulations. The possible structures of CD10 could be described by the flip of glucose subunits on its macro-ring. The results revealed that the CD10 structures preferred to form in the saddle-like shape with two flips at the opposite bending positions like the X-ray structure. The flip from *cis*- to *trans*-position of a glucose in the CD10 ring was subject to the flat conformation. Next,

the study of CD14 conformations were also conducted with the same validated REMD condition as CD10. The conformation study was performed by new structural analysis: biplanar angle and circularity. The CD14 structures still remain in the bent form, but are slightly more open than in its crystal structure. Interestingly, the 2-loop structure could be formed for the CD14. Additionally, it is possible to get some insight into the temperature dependence of conformational changes. Increase of energy content due to elevated temperatures is tightly correlated with an increase of diversity of various conformations of the macrocycle. These finding might be also useful in the temperature-controlled synthesis of LR-CDs as well as other experimental conditions, in particular for the host-guest reaction.

Second, based on the microsecond timescale simulations of the β CD molecule in lipid bilayer, we found that the β CD molecule spontaneously permeated toward the lipid surface, but did not further translocate into bilayer's tail region. The physical damage of bilayer could not be observed when the β CD molecule attached to the bilayer surface, in contrast the water pore formation in lipid bilayer occurred when the β CD molecule stayed inside the bilayer. The simulation results also showed that the secondary rim of the β CD molecule was the main contribution for the β CD-lipid interactions in which strong hydrogen bond formation between the secondary rim and lipid heads were always found for the whole length of the simulation time. Interestingly, the conformations of the β CD molecule changed at various solvation phases (water, water-bilayer interface and bilayer) due to the loss of the intramolecular hydrogen bonds and an enlargement of the area cavity of the water-bilayer interface could be observed. Moreover, the influence on the membrane permeability of modified β CDs as

ME β CD and HP β CD derivatives were considered according to their chemical function and substitution positions of methoxy groups and 2-hydroxypropyl groups at 2-, 6, and 2,6-position of hydroxyl groups on regular β CD. The significant differences of the permeation depth between the β CD derivatives and non-modified β CD were investigated. The approaching of the wider rim likely induced the deeper permeation of β CD derivatives. As well as the long chain substitution of 2-hydroxypropyl at 2,6-position resulted in the deepest permeation. These findings might be related to drug delivery of these β CD derivatives.



REFERENCES

1. Brocos, P., et al., *Similarities and differences between cyclodextrin-sodium dodecyl sulfate host-guest complexes of different stoichiometries: molecular dynamics simulations at several temperatures*. The Journal of Physical Chemistry B, 2010. **114**(39): p. 12455-12467.
2. Ueda, H., *Physicochemical Properties and Complex Formation Abilities of Large-Ring Cyclodextrins*. Journal of Inclusion Phenomena and Macrocyclic Chemistry, 2002. **44**(1-4): p. 53-56.
3. Ueda, H., *Large ring cyclodextrins-recent progress*. FABAD Journal of Pharmaceutical Sciences, 2004. **29**: p. 27-38.
4. Bennett, W.F.D. and D.P. Tieleman, *Water defect and pore formation in atomistic and coarse-grained lipid membranes: pushing the limits of coarse graining*. Journal of Chemical Theory and Computation, 2011. **7**(9): p. 2981-2988.
5. Betzel, C., et al., *Topography of cyclodextrin inclusion complexes, part 20. circular and flip-flop hydrogen bonding in .beta.-cyclodextrin undecahydrate: a neutron diffraction study*. Journal of the American Chemical Society, 1984. **106**(24): p. 7545-7557.
6. Harata, K., *The structure of the cyclodextrin complex. XX. crystal structure of uncomplexed hydrated γ-cyclodextrin*. Bulletin of the Chemical Society of Japan, 1987. **60**(8): p. 2763-2767.
7. Kurkov, S.V. and T. Loftsson, *Cyclodextrins*. International Journal of Pharmaceutics, 2013. **453**(1): p. 167-180.

8. Loftsson, T., et al., *Cyclodextrins in drug delivery*. Expert Opinion on Drug Delivery, 2005. **2**(2): p. 335-351.
9. VanEtten, R.L., et al., *The mechanism of the cycloamylose-accelerated cleavage of phenyl esters*. Journal of the American Chemical Society, 1967. **89**(13): p. 3253-3262.
10. Tabushi, I., et al., *Specific inclusion catalysis by .beta.-cyclodextrin in the one-step preparation of vitamin K1 or K2 analogs*. Journal of the American Chemical Society, 1979. **101**(4): p. 1019-1026.
11. Al-Rawashdeh, N.A.F., K.S. Al-Sadeh, and M.B. Al-Bitar, *Inclusion complexes of sunscreen agents with β -cyclodextrin: spectroscopic and molecular modeling studies*. Journal of Spectroscopy, 2013. **2013**: p. 11.
12. Cramer, F., W. Saenger, and H.C. Spatz, *Inclusion compounds. XIX.1a the formation of inclusion compounds of α -cyclodextrin in aqueous solutions. thermodynamics and kinetics*. Journal of the American Chemical Society, 1967. **89**(1): p. 14-20.
13. Nathir, A.F.A.-R., S.A.-S. Khaled, and A.-B. Mohammad Bassam, *Inclusion complexes of sunscreen agents with β -cyclodextrin: spectroscopic and molecular modeling studies*. Journal of Spectroscopy, 2013. **2013**.
14. Kano, K., et al., *Static and dynamic behavior of 2:1 inclusion complexes of cyclodextrins and charged porphyrins in aqueous organic media*. Journal of the American Chemical Society, 2002. **124**(33): p. 9937-9944.
15. Suzuki, M., et al., *The association of inclusion complexes of cyclodextrins with azo dyes*. Journal of Inclusion Phenomena and Molecular Recognition in Chemistry, 1994. **18**(3): p. 255-264.

16. Grosse, P.Y., F. Bressolle, and F. Pinguet, *In vitro modulation of doxorubicin and docetaxel antitumoral activity by methyl- β -cyclodextrin*. European Journal of Cancer, 1998. **34**(1): p. 168-174.
17. Lipinski, C.A., et al., *Experimental and computational approaches to estimate solubility and permeability in drug discovery and development settings*. Advanced Drug Delivery Reviews, 2001. **46**(1–3): p. 3-26.
18. Amidon, G.L., et al., *A theoretical basis for a biopharmaceutic drug classification: the correlation of in vitro drug product dissolution and in vivo bioavailability*. Pharmaceutical Research, 1995. **12**(3): p. 413-20.
19. Tommasini, S., et al., *Improvement in solubility and dissolution rate of flavonoids by complexation with beta-cyclodextrin*. Journal of Pharmaceutical and Biomedical Analysis, 2004. **35**(2): p. 379-387.
20. Jullian, C., et al., *Complexation of quercetin with three kinds of cyclodextrins: An antioxidant study*. Spectrochimica Acta Part A: Molecular and Biomolecular Spectroscopy, 2007. **67**(1): p. 230-234.
21. Merkus, F.W.H.M., et al., *Cyclodextrins in nasal drug delivery*. Advanced Drug Delivery Reviews, 1999. **36**(1): p. 41-57.
22. Hirayama, F. and K. Uekama, *Cyclodextrin-based controlled drug release system*. Advanced Drug Delivery Reviews, 1999. **36**(1): p. 125-141.
23. Abi-Mosleh, L., et al., *Cyclodextrin overcomes deficient lysosome-to-endoplasmic reticulum transport of cholesterol in Niemann-Pick type C cells*. Proceedings of the National Academy of Sciences of the United States of America, 2009. **106**(46): p. 19316-19321.

24. López, C.A., A.H. de Vries, and S.J. Marrink, *Molecular mechanism of cyclodextrin mediated cholesterol extraction*. PLOS Computational Biology, 2011. **7**(3): p. e1002020.
25. Cesar, A.L., H.d.V. Alex, and J.M. Siewert, *Computational microscopy of cyclodextrin mediated cholesterol extraction from lipid model membranes*. Scientific Reports, 2013. **3**.
26. Ueda, H., et al., *Isolation, purification, and characterization of cyclomaltoodecaose (ϵ -CD)*. Journal of Inclusion Phenomena and Macrocyclic Chemistry, 1996. **25**(1-3): p. 17-20.
27. Jacob, J., et al., *Band-flip and kink as novel structural motifs in α -(1-4)-D-glucose oligosaccharides. Crystal structures of cyclodeca- and cyclotetradecaamylose*. Carbohydrate Research, 1999. **322**(3): p. 228-246.
28. Harata, K., et al., *X-Ray Structure of α -cyclodextrin*. Supramolecular Chemistry, 1998. **9**(2): p. 143-150.
29. Jacob, J., et al., *Strain-induced "band flips" in cyclodecaamylose and higher homologues*. Angewandte Chemie International Edition, 1998. **37**(5): p. 605-609.
30. Nimz, O., et al., *An orthorhombic crystal form of cyclohexaicosaoose, CA26·32.59 H₂O: comparison with the triclinic form*. Carbohydrate research, 2001. **336**(2): p. 141-153.
31. Gessler, K., et al., *V-Amylose at atomic resolution: X-ray structure of a cycloamylose with 26 glucose residues (cyclomaltohexaicosaoose)*. Proceedings of the National Academy of Sciences, 1999. **96**(8): p. 4246-4251.

32. Chacko, K.K. and W. Saenger, *Topography of cyclodextrin inclusion complexes. 15. crystal and molecular structure of the cyclohexaamylose-7.57 water complex, form III. four- and six-membered circular hydrogen bonds.* Journal of the American Chemical Society, 1981. **103**(7): p. 1708-1715.
33. French, D., Pulley, A.O., Effenberger, J.A., Rougvie, M.A., Abdullah, M., Archives of Biochemistry and Biophysics, 1965. **111**: p. 153-160.
34. Gotsev, M.G. and P.M. Ivanov, *Large-ring cyclodextrins. A molecular dynamics study of the conformational dynamics and energetics of CD10, CD14 and CD26.* ARKIVOC, 2007. **13**: p. 167-189.
35. Machida, S., et al., *Cycloamylose as an efficient artificial chaperone for protein refolding.* FEBS Letters, 2000. **486**(2): p. 131-135.
36. Qi, Q., et al., *Effect of the reaction temperature on the transglycosylation reactions catalyzed by the cyclodextrin glucanotransferase from Bacillus macerans for the synthesis of large-ring cyclodextrins.* Tetrahedron, 2004. **60**(3): p. 799-806.
37. Qi, Q., M. Mokhtar, and W. Zimmermann, *Effect of ethanol on the synthesis of large-ring cyclodextrins by cyclodextrin glucanotransferases.* Journal of Inclusion Phenomena and Macrocyclic Chemistry, 2007. **57**(1-4): p. 95-99.
38. Shimada, J., et al., *Conformation of novel cycloamylose: topological aspects and simulations.* Macromolecules, 1996. **29**(20): p. 6408-6421.
39. Shimada, J., et al., *Conformation of amylose in aqueous solution: small-angle x-ray scattering measurements and simulations.* The Journal of Physical Chemistry B, 2000. **104**(9): p. 2136-2147.

40. Ivanov, P.M. and C. Jaime, *Insights into the structure of large-ring cyclodextrins through molecular dynamics simulations in solution*. The Journal of Physical Chemistry B, 2004. **108**(20): p. 6261-6274.
41. Maestre, I., et al., *Structural dynamics of some large-ring cyclodextrins. A molecular dynamics study: an analysis of force field performance*. Theoretical Chemistry Accounts, 2007. **117**(1): p. 85-97.
42. Gotsev, M.G. and P.M. Ivanov, *Large-ring cyclodextrins. Further support for the preferred conformations of CD26 in water solution: molecular dynamics studies on CD26-derived conformations of CD_n (n = 24, 25, 27, 28, 29, 30)*. International Journal of Quantum Chemistry, 2007. **107**(8): p. 1657-1672.
43. Gotsev, M.G., P.M. Ivanov, and C. Jaime, *Molecular dynamics study of the conformational dynamics and energetics of some large-ring cyclodextrins (CD_n, n = 24, 25, 26, 27, 28, 29)*. Chirality, 2007. **19**(3): p. 203-213.
44. Gotsev, M.G. and P.M. Ivanov, *Molecular dynamics of large-ring cyclodextrins: principal component analysis of the conformational interconversions*. The Journal of Physical Chemistry B, 2009. **113**(17): p. 5752-5759.
45. Ivanov, P.M., *Computational studies on the conformations of some large-ring cyclodextrins (CD_n, n= 20, 21, 22, 23)*. Chirality, 2011. **23**(8): p. 628-637.
46. Ivanov, P., *Conformations of some lower-size large-ring cyclodextrins derived from conformational search with molecular dynamics and principal component analysis*. Journal of Molecular Structure, 2012. **1009**: p. 3-10.

47. Spooner, M.J. and P.A. Gale, *Anion transport across varying lipid membranes-the effect of lipophilicity*. *Chemical Communications* 2015. **51**(23): p. 4883-4886.
48. Berendsen, H.J.C., D. van der Spoel, and R. Vandrunen, *Gromacs - a message-passing parallel molecular-dynamics implementation*. *Computer Physics Communications*, 1995. **91**(1-3): p. 43-56.
49. Hess, B., et al., *GROMACS 4: Algorithms for highly efficient, load-balanced, and scalable molecular simulation*. *Journal of Chemical Theory and Computation*, 2008. **4**(3): p. 435-447.
50. Pronk, S., et al., *GROMACS 4.5: a high-throughput and highly parallel open source molecular simulation toolkit*. *Bioinformatics*, 2013. **29**(7): p. 845-854.
51. Oostenbrink, C., et al., *A biomolecular force field based on the free enthalpy of hydration and solvation: The GROMOS force-field parameter sets 53A5 and 53A6*. *Journal of Computational Chemistry*, 2004. **25**(13): p. 1656-1676.
52. Wang, J., P. Cieplak, and P.A. Kollman, *How well does a restrained electrostatic potential (RESP) model perform in calculating conformational energies of organic and biological molecules?* *Journal of Computational Chemistry*, 2000. **21**(12): p. 1049-1074.
53. Feller, S.E. and A.D. MacKerell, *An improved empirical potential energy function for molecular simulations of phospholipids*. *The Journal of Physical Chemistry B*, 2000. **104**(31): p. 7510-7515.
54. Soares, T.A., et al., *An improved nucleic acid parameter set for the GROMOS force field*. *Journal of Computational Chemistry*, 2005. **26**(7): p. 725-737.

55. Salvatierra, D., et al., *Determination of the inclusion geometry for the beta-cyclodextrin benzoic acid complex by NMR and molecular modeling*. Journal of Organic Chemistry, 1996. **61**(26): p. 9578-9581.
56. Heiner, A.P., J. Sugiyama, and O. Teleman, *Crystalline cellulose I alpha and I beta studied by molecular dynamics simulation*. Carbohydrate Research, 1995. **273**(2): p. 207-223.
57. Bonnet, P., C. Jaime, and L. Morin-Allory, *alpha, beta, and gamma-cyclodextrin dimers. Molecular modeling studies by molecular mechanics and molecular dynamics simulations*. Journal of Organic Chemistry, 2001. **66**(3): p. 689-692.
58. Yu, Y.M., et al., *Molecular dynamics study of the inclusion of cholesterol into cyclodextrins*. The Journal of Physical Chemistry B, 2006. **110**(12): p. 6372-6378.
59. Feng, T., et al., *Application of molecular dynamics simulation in food carbohydrate research-a review*. Innovative Food Science & Emerging Technologies, 2015. **31**: p. 1-13.
60. Shi, M., et al., *Stereoselective inclusion mechanism of ketoprofen into beta-cyclodextrin: insights from molecular dynamics simulations and free energy calculations*. Theoretical Chemistry Accounts, 2014. **133**(10).
61. Alvira, E., *Theoretical study of the separation of valine enantiomers by beta-cyclodextrin with different solvents: a molecular mechanics and dynamics simulation*. Tetrahedron-Asymmetry, 2015. **26**(15-16): p. 853-860.
62. Cao, R. and S. Wu, *In silico properties characterization of water-soluble gamma-cyclodextrin bi-capped C-60 complex: Free energy and geometrical*

- insights for stability and solubility*. Carbohydrate Polymers, 2015. **124**: p. 188-195.
63. Dodziuk, H. and O. Lukin, *Modelling of molecular and chiral recognition by cyclodextrins. Is it reliable? Part 2. molecular dynamics calculations in vacuum pertaining to the selective complexation of decalins by beta-cyclodextrin*. Polish Journal of Chemistry, 2000. **74**(7): p. 997-1001.
64. Terekhova, I.V., et al., *Selective Na⁺/K⁺ effects on the formation of alpha-cyclodextrin complexes with aromatic carboxylic acids: competition for the guest*. The Journal of Physical Chemistry B, 2010. **114**(39): p. 12607-12613.
65. Figueiras, A., et al., *Molecular interaction governing solubility and release profiles in supramolecular systems containing fenbufen, pluronics and cyclodextrins*. Journal of Inclusion Phenomena and Macrocyclic Chemistry, 2015. **81**(3-4): p. 395-407.
66. Zhang, H.Y., et al., *Insight into the structural deformations of beta-Cyclodextrin caused by alcohol cosolvents and guest Molecules*. The Journal of Physical Chemistry B, 2012. **116**(12): p. 3880-3889.
67. Deol, S.S., et al., *Lipid-protein interactions of integral membrane proteins: a comparative simulation study*. Biophysical journal, 2004. **87**(6): p. 3737-3749.
68. Gumbart, J., et al., *Molecular dynamics simulations of proteins in lipid bilayers*. Current Opinion in Structural Biology, 2005. **15**(4): p. 423-431.
69. Hansmann, U.H., *Parallel tempering algorithm for conformational studies of biological molecules*. Chemical Physics Letters, 1997. **281**(1): p. 140-150.
70. Sugita, Y. and Y. Okamoto, *Replica-exchange molecular dynamics method for protein folding*. Chemical Physics Letters, 1999. **314**(1-2): p. 141-151.

71. Nymeyer, H., S. Gnanakaran, and A.E. Garcia, *Atomic simulations of protein folding, using the replica exchange algorithm*. *Methods in Enzymology*, 2004. **383**: p. 119-149.
72. Cheng, X., et al., *Modified replica exchange simulation methods for local structure refinement*. *The Journal of Physical Chemistry B*, 2005. **109**(16): p. 8220-8230.
73. Kamberaj, H. and A. van der Vaart, *Multiple scaling replica exchange for the conformational sampling of biomolecules in explicit water*. *Journal of Chemical Physics*, 2007. **127**(23).
74. Okumura, H., E. Gallicchio, and R.M. Levy, *Conformational populations of ligand-sized molecules by replica exchange molecular dynamics and temperature reweighting*. *Journal of Computational Chemistry*, 2010. **31**(7): p. 1357-1367.
75. van der Spoel, D., et al., *GROMACS User Manual*. 1991-2005.
76. Tieleman, D.P., S.J. Marrink, and H.J.C. Berendsen, *A computer perspective of membranes: molecular dynamics studies of lipid bilayer systems*. *Biochimica Et Biophysica Acta-Reviews on Biomembranes*, 1997. **1331**(3): p. 235-270.
77. Brooks III, C.L., M. Karplus, and B.M. Pettitt, *Proteins: a theoretical perspective of dynamics, structure and thermodynamics*. 1988, New York: John Wiley & Sons.
78. Allen, M.P. and D.J. Tildesley, *Computer simulation of liquids*. . 1987, Oxford: Clarendon Press.
79. Leach, A.R., *Molecular modelling. Principles and applications*. 1996, Singapore: Addison Wesley Longman Limited.

80. Jacob, J., et al., *Strain-induced "band flips" in cyclodecaamylose and higher homologues*. *Angew. Chem. Int. Edit*, 1998. **37**(5): p. 605-609.
81. Fujiwara, T., N. Tanaka, and S. Kobayashi, *Structure of δ -cyclodextrin•13.75 H₂O*. *Chemistry Letters*, 1990. **19**(5): p. 739-742.
82. Kirschner, K.N. and R.J. Woods, *Solvent interactions determine carbohydrate conformation*. *Proceedings of the National Academy of Sciences of the United States of America*, 2001. **98**(19): p. 10541-10545.
83. Basma, M., et al., *Solvated ensemble averaging in the calculation of partial atomic charges*. *Journal of Computational Chemistry*, 2001. **22**(11): p. 1125-37.
84. Kirschner, K.N. and R.J. Woods, *Quantum mechanical study of the nonbonded forces in water-methanol complexes*. *The Journal of Physical Chemistry A*, 2001. **105**(16): p. 4150-4155.
85. Kirschner, K.N., et al., *GLYCAM06: a generalizable biomolecular force field. Carbohydrates*. *Journal of Computational Chemistry*, 2008. **29**(4): p. 622-655.
86. Tessier, M.B., et al., *Extension of the GLYCAM06 biomolecular force field to lipids, lipid bilayers and glycolipids*. *Molecular Simulation*, 2008. **34**(4): p. 349-363.
87. Nutho, B., et al., *Binding mode and free energy prediction of fisetin/ β -cyclodextrin inclusion complexes*. *Beilstein Journal of Organic Chemistry*, 2014. **10**: p. 2789-2799.
88. Sangpheak, W., et al., *Enhanced stability of a naringenin/2,6-dimethyl β -cyclodextrin inclusion complex: Molecular dynamics and free energy*

- calculations based on MM- and QM-PBSA/GBSA.* Journal of Molecular Graphics and Modelling, 2014. **50**(0): p. 10-15.
89. Cezard, C., et al., *Molecular dynamics studies of native and substituted cyclodextrins in different media: 1. charge derivation and force field performances.* Physical Chemistry Chemical Physics, 2011. **13**(33): p. 15103-15121.
90. Rungnim, C., et al., *Replica exchange molecular dynamics simulation of chitosan for drug delivery system based on carbon nanotube.* Journal of Molecular Graphics & Modelling, 2013. **39**: p. 183-192.
91. Snor, W., et al., *On the structure of anhydrous β -cyclodextrin.* Chemical Physics Letters, 2007. **441**(1-3): p. 159-162.
92. Pourmousa, M., et al., *Molecular dynamic studies of transportan interacting with a DPPC lipid bilayer.* The Journal of Physical Chemistry B, 2013. **117**(1): p. 230-241.
93. Karami, L. and S. Jalili, *Effects of cholesterol concentration on the interaction of cytarabine with lipid membranes: a molecular dynamics simulation study.* Journal of Biomolecular Structure & Dynamics, 2015. **33**(6): p. 1254-1268.
94. Lins, R.D. and P.H. Hunenberger, *A new GROMOS force field for hexopyranose-based carbohydrates.* Journal of Computational Chemistry 2005. **26**(13): p. 1400-1412.
95. Berger, O., O. Edholm, and F. Jähnig, *Molecular dynamics simulations of a fluid bilayer of dipalmitoylphosphatidylcholine at full hydration, constant pressure, and constant temperature.* Biophysical Journal, 1997. **72**(5): p. 2002-2013.

96. Tieleman, D.P. and H.J. Berendsen, *A molecular dynamics study of the pores formed by Escherichia coli OmpF porin in a fully hydrated palmitoylphosphatidylcholine bilayer*. Biophysical Journal, 1998. **74**(6): p. 2786-801.
97. Berendsen, H.J.C., et al., *Interaction models for water in relation to protein hydration*, in *Intermolecular Forces*, B. Pullman, Editor. 1981, Springer Netherlands. p. 331-342.
98. Bussi, G., D. Donadio, and M. Parrinello, *Canonical sampling through velocity rescaling*. The Journal of chemical physics, 2007. **126**(1): p. 014101.
99. Bussi, G., T. Zykova-Timan, and M. Parrinello, *Isothermal-isobaric molecular dynamics using stochastic velocity rescaling*. The Journal of chemical physics, 2009. **130**(7): p. 074101.
100. Berendsen, H.J.C., et al., *Molecular-dynamics with coupling to an external bath*. Journal of Chemical Physics, 1984. **81**(8): p. 3684-3690.
101. Darden, T., D. York, and L. Pedersen, *Particle mesh Ewald: An $N \cdot \log(N)$ method for Ewald sums in large systems*. The Journal of chemical physics, 1993. **98**(12): p. 10089-10092.
102. Essmann, U., et al., *A smooth particle mesh Ewald method*. The Journal of Chemical Physics, 1995. **103**(19): p. 8577-8593.
103. Karttunen, M., et al., *Electrostatics in biomolecular simulations: Where are we now and where are we heading?* Current Topics in Membranes, 2008. **60**: p. 49-89.
104. Hess, B., et al., *LINCS: A linear constraint solver for molecular simulations*. Journal of Computational Chemistry, 1997. **18**(12): p. 1463-1472.

105. Cino, E.A., W.Y. Choy, and M. Karttunen, *Comparison of secondary structure formation using 10 different force fields in microsecond molecular dynamics simulations*. Journal of Chemical Theory and Computation, 2012. **8**(8): p. 2725-2740.
106. Wong-Ekkabut, J. and M. Karttunen, *Assessment of common simulation protocols for simulations of nanopores, membrane proteins, and channels*. Journal of Chemical Theory and Computation, 2012. **8**(8): p. 2905-2911.
107. Humphrey, W., A. Dalke, and K. Schulten, *VMD: visual molecular dynamics*. Journal of Molecular Graphics, 1996. **14**(1): p. 33-38.
108. van der Spoel, D. and M.M. Seibert, *Protein folding kinetics and thermodynamics from atomistic simulations*. Physical Review Letters, 2006. **96**(23): p. 238102.
109. Okumura, H., *Temperature and pressure denaturation of chignolin: Folding and unfolding simulation by multibaric-multithermal molecular dynamics method*. Proteins: Structure, Function, and Bioinformatics, 2012. **80**(10): p. 2397-2416.
110. Khuntawee, W., et al., *Conformation study of ϵ -cyclodextrin: replica exchange molecular dynamics simulations*. Carbohydrate Polymers, 2015. **in press**.
111. Mascetti, J., et al., *Organization of β -cyclodextrin under pure cholesterol, DMPC, or DMPG and mixed cholesterol/phospholipid monolayers*. Langmuir, 2008. **24**(17): p. 9616-9622.
112. López, C.A., A.H. de Vries, and S.J. Marrink, *Computational microscopy of cyclodextrin mediated cholesterol extraction from lipid model membranes*. Scientific reports, 2013. **3**.

113. Lukat, G., J. Krüger, and B. Sommer, *APL@Voro: A voronoi-based membrane analysis tool for GROMACS trajectories*. *Journal of Chemical Information and Modeling*, 2013. **53**(11): p. 2908-2925.
114. Dodziuk, H., *Cyclodextrins and their complexes: chemistry, analytical methods, applications*. 2006: John Wiley & Sons.
115. Yong, C.W., C. Washington, and W. Smith, *Structural behaviour of 2-hydroxypropyl- β -cyclodextrin in water: molecular dynamics simulation studies*. *Pharmaceutical research*, 2008. **25**(5): p. 1092-1099.
116. Koehler, J.E.H., W. Saenger, and W.F. van Gunsteren, *The flip-flop hydrogen bonding phenomenon*. *European Biophysics Journal*, 1988. **16**(3): p. 153-168.
117. Saenger, W., et al., *Structures of the common cyclodextrins and their larger analogues-beyond the doughnut*. *Chemical Reviews*, 1998. **98**(5): p. 1787-1802.
118. Koehler, J., W. Saenger, and W. Van Gunsteren, *Molecular dynamics simulation of crystalline β -cyclodextrin dodecahydrate at 293 K and 120 K*. *European Biophysics Journal*, 1987. **15**(4): p. 211-224.

APPENDIX



จุฬาลงกรณ์มหาวิทยาลัย
CHULALONGKORN UNIVERSITY

Publications related to thesis topic

[1] **Khuntawee, W.**, Wolschann, P., Rungrotmongkol, T., Wong-Ekkabut, J., Hannongbua, S. Molecular dynamics simulations of the interaction of beta cyclodextrin with lipid bilayer. *Journal of Chemical Information and Modeling*. 2015, DOI: 10.1021/acs.jcim.5b00152

[2] **Khuntawee, W.**, Rungrotmongkol, T., Wolschann, P., Pongsawasdi, P., Kungwan, N., Okumura, H., Hannongbua, S. Conformation Study of <epsilon>-Cyclodextrin: Replica Exchange Molecular Dynamics Simulations. *Carbohydrate Polymers*. 2015, *in press*

Selected training and conference activity

W. Khuntawee, J. Wong-ekkabut, T. Rungrotmongkol, P. Wolschann and S. Hannongbua. Permeation mechanism of beta cyclodextrin and its derivatives into cell membrane for drug delivery application, the 18th International Annual Symposium on Computational Science and Engineering (ANSCSE18) Kasetsart University, Si Racha Campus, Chonburi, Thailand, March 17-19, 2014 (Oral presentation)

W. Khuntawee, T. Rungrotmongkol, P. Wolschann, J. Wong-ekkabut and S. Hannongbua. The permeation behavior of beta cyclodextrin through lipid bilayer, 2014 International Biophysics Congress Brisbane Convention and Exhibition Centre, Brisbane, Queensland, Australia August 3-7, 2014 (Poster presentation)

W. Khuntawee, T. Rungrotmongkol, P. Wolschann, H. Okumura, M. Kunaseth, C. Rungnim and S. Hannongbua. The Conformation Study of Large Ring Cyclodextrin: Replica Exchange Molecular Dynamics Simulations, The 11th-Thai Summer School of Computational Chemistry (11th-TS2C2) Nan, Thailand, January 4-7, 2015 (Poster presentation)



VITA

Name	Wasinee Khuntawee
Nationality	Thai
Date of birth	February 15th, 1987
E-mail address	w.khuntawee@gmail.com
Education	
2010-2015	Doctor of Philosophy (Ph.D.) in Nanoscience and Technology Graduate School, Chulalongkorn University, Bangkok, Thailand
2009-2010	Master of Science degree (M.Sc.) in Chemistry Faculty of Science, Chulalongkorn University, Bangkok, Thailand
2005-2009	Bachelor of Science degree (B.Sc.) in Chemistry Faculty of Science, Silpakorn University, Nakhon Pathom, Thailand

I majored in Chemistry, Faculty of Science, Silpakorn University. There I had an experience in textile technology during my undergraduate years and completed my Bachelor degree. Then I earned a Master degree in Physical Chemistry from Chulalongkorn University. I was motivated to study biological interests using several computer simulation techniques. So far I have held a doctor of Philosophy degree in Nanoscience and Technology program, Chulalongkorn University. My works have been presented in many scientific conferences and successfully published in seven internationally notable publications. In addition, I have gained a great number of aboard experiences. Two of my precious aboard experiences are being a six-month exchange student under JASSO Scholarship visiting Institute for Molecular Science (IMS), Okazaki, Japan and being two-month exchange student under OeAD scholarship visiting Department of Pharmaceutical Technology and Biopharmaceutics, University of Vienna, Austria. As an exchange student under the supervision of Assoc. Prof. Dr. Hisashi Okumura, Department of Structural Molecular Science, The Graduate University for Advanced Studies in Japan, I had a great opportunity to visit his laboratory and learned from his instruction in particular the replica exchange MD method. In Austria, Prof. Dr. Peter Wolschann, Department of Pharmaceutical Technology and Biopharmaceutics, University of Vienna, gave me beneficial suggestions about cyclodextrin research.